Article

Design and Synthesis of Novel 5-((3-(Trifluoromethyl)piperidin-1-yl)sulfonyl)indoline-2,3-dione Derivatives as Promising Antiviral Agents: In Vitro, In Silico, and Structure–Activity Relationship Studies

Rogy R. Ezz Eldin [1,*], Marwa A. Saleh [2], Sefat A. Alwarsh [3], Areej Rushdi [4], Azza Ali Althoqapy [4], Hoda S. El Saeed [2] and Ayman Abo Elmaaty [5,*]

[1] Pharmaceutical Organic Chemistry Department, Faculty of Pharmacy, Port Said University, Port Said 42526, Egypt
[2] Pharmaceutical Organic Chemistry Department, Faculty of Pharmacy (Girls), Al-Azhar University, Cairo 11651, Egypt; marwasaleh577@yahoo.com (M.A.S.); hodasamir3185@gmail.com (H.S.E.S.)
[3] Department of Science, Prince Sultan Military College of Health Sciences, Dhahran 31932, Saudi Arabia; salwarsh@psmchs.edu.sa
[4] Department of Medical Microbiology and Immunology, Faculty of Medicine for Girls, Al-Azhar University, Cairo 11651, Egypt; areejrushdi@azhar.edu.eg (A.R.); azzaaly.micro@azhar.edu.eg (A.A.A.)
[5] Medicinal Chemistry Department, Faculty of Pharmacy, Port Said University, Port Said 42526, Egypt
[*] Correspondence: rogyezz29@gmail.com (R.R.E.E.); ayman.mohamed@pharm.psu.edu.eg (A.A.E.)

Abstract: Herein, a series of new isatin derivatives was designed and synthesized (**1–9**) as broad-spectrum antiviral agents. Consequently, the antiviral activities of the synthesized compounds (**1–9**) were pursued against three viruses, namely influenza virus (H1N1), herpes simplex virus 1 (HSV-1), and coxsackievirus B3 (COX-B3). In particular, compounds **9**, **5**, and **4** displayed the highest antiviral activity against H1N1, HSV-1, and COX-B3 with IC_{50} values of 0.0027, 0.0022, and 0.0092 μM, respectively. Compound **7** was the safest, with a CC_{50} value of 315,578.68 μM. Moreover, a quantitative PCR (real-time PCR) assay was carried out for the most relevant compounds. The selected compounds exhibited a decrease in viral gene expression. Additionally, the conducted in silico studies emphasized the binding affinities of the synthesized compounds and their reliable pharmacokinetic properties as well. Finally, a structure–antiviral activity relationship study was conducted to anticipate the antiviral activity change upon future structural modification.

Keywords: isatin; H1N1; HSV-1; coxsackievirus B3; qPCR

1. Introduction

Viruses are considered pathogens that cause a lot of diseases, varying from self-healing diseases to acute fatal diseases [1]. SARS-CoV-2-mediated COVID-19 progression made it one of the most perplexing pandemics in the history of mankind. As of 20 April 2022, more than 504.4 million reported COVID-19 cases and more than 6.2 million related deaths have been reported by the WHO, and in early 2022, nearly 1.2 million new cases were being estimated every day [2,3]. In 2019, the WHO reported that 296 million people were suffering from chronic hepatitis B infections. From this number, about 1.5 million people were reported as new cases of the virus in 2019 [3]. Additionally, worldwide infections with human immunodeficiency virus (HIV) rose to about 37.7 million by the year 2020 [3]. Additionally, infections caused by the herpes simplex virus (HSV) are considered one of the most common viral infections [4]. Lately, infections caused by the herpes simplex virus (HSV-1) have exceeded 80% of the human population [5]. Firstly, HSV-1 infects mucosal epithelial cells, establishing a long-term infection in sensory neurons. Then, HSV-1 re-activation results in the formation of painful, vesicular lesions in the oral–facial area [5],

particularly in elderly and immunocompromised people, leading to dangerous diseases, such as herpes encephalitis, and blindness due to keratitis [5,6]. Acyclic nucleosides, such as acyclovir, ganciclovir, and penciclovir, are the most widely used drugs as anti-herpes agents [7]. Coxsackievirus B3 (Cox B3) belongs to the Picornaviridae family, which is composed of single-stranded positive-sense RNA viruses [8]. Coxsackievirus B3 (Cox B3) infects neonates in their first week, causing severe illnesses such as myocarditis or meningoencephalitis [9]. Benserazide was found to be the first inhibitor against coxsackievirus B3 [10]. Currently, the world still lacks effective therapies for viral infections. There is a great need for the further development of antiviral drug design and refinement strategies for combating viral infections because the currently used treatments are not effective enough and are not well tolerated [11].

We cannot ignore the success of vaccines in the eradication of important viral pathogens, such as measles, rubella, mumps, smallpox, and polio. But, the vaccine approaches for viruses such as human immunodeficiency virus (HIV) and hepatitis C virus (HCV) are still not sufficient [11,12].

The first mass vaccination campaigns against SARS-CoV-2 were available only 38 weeks after the declaration of the COVID-19 pandemic by the WHO in March 2020. As of 6 May 2022, a total of 10 vaccine products have been approved by the WHO for emergency use [3]. Also, there are great efforts for HCV vaccine development [13]. Recently, the inhalation of dry powder vaccine for respiratory viruses has been considered a new approach, exhibiting convincing efficacy and high safety comparable to the parenteral administration route [14].

Also, in 2009, the world faced a pandemic caused by influenza virus H1N1 attacks. The H1N1 infection was transmitted very quickly in both children and adults, leading to respiratory symptoms ranging from self-limited to complicated cases characterized by pneumonia and acute respiratory distress that needed hospitalization [15,16].

Moreover, in order to understand the different approaches that have been developed to design antiviral agents, the viral replication cycle should be clear. The viral replication cycle of some viruses involves the following stages: (1) the attachment and adsorption of the virus to the host cell, (2) the reprogramming of the host cell DNA machinery to synthesize the viral genome, and (3) virion assembly and exocytosis [17–21].

On the other hand, drugs that combat viral infections are called antiviral drugs. In principle, antiviral drugs target either viral proteins or cellular proteins [11]. Antiviral drugs could be classified as inhibitors of viral adsorption (polysulphates, polysulphonates), inhibitors of virus cell fusion (HIV: AMD3100, TAK779), uncoating inhibitors, neuroaminidase inhibitors (zanamivir, oseltamivir), inhibitors of integrase (raltegravir), protease inhibitors (ritonavir, atazanavir, and darunavir), viral DNA polymerase inhibitors (acyclovir, tenofovir, valganciclovir, and valacyclovir), and reverse transcriptase inhibitors (emtricitabine, amdoxovir for HIV) [11,22].

It is worth mentioning that, according to the genetic literature, there are two types of viruses: DNA and RNA viruses. Owing to their ability to integrate with the host cell genetic material, targeting RNA viruses and controlling them is challenging. Additionally, RNA viruses keep high mutation rates, further complicating the case; so, RNA-dependent RNA polymerases (RdRps) remain among the most critical viral drug targets [22]. Some RdRps have been approved by the FDA, e.g., remdesivir for COVID-19 and Ebola treatment and ribavirin and dasabuvir for hepatitis C treatment, as well as favipiravir for influenza virus treatment [22,23].

Furthermore, broad-spectrum antiviral agents (BSAAs) are compounds that target the viruses of two or more viral families, among which hydroxychloroquine, imatinib, and ribavirin could provide additional protection from emerging and viral diseases. BSAAs are usually combined with other antiviral drugs, resulting in synergistic or additive effects against viral infection [24]. Moreover, several plant-derived active constituents have been reported to possess interesting antiviral activities, including polyphenols, which played beneficial roles in the immune homeostasis for COVID-19 treatment [25], as well

as flavonols, which have been proven to be potent antiviral agents targeting SARS-CoV-2 proteases [26].

Over the past five decades, isatin, an indole analog, has been described as a broad-spectrum antiviral agent emphasized in structure–activity relationship (SAR) studies [27]. For example, isatin–pyrimidinone hybrids and naphthyl-2-methyl isatin derivatives were found to be equally or more potent than the standards used in fighting HIV and SARS-CoV-2, with IC_{50} values of 0.0742 and 0.045 μM (compounds I and II, respectively), as shown in Figure 1 [27]. Also, isatin sulphonamide derivatives possessed a binding affinity of −9.6 kcal/mol within the active site of the NSP3 receptor of SARS-CoV-2 [28]. Additionally, two isatin–oxadiazole hybrids exhibited enhanced activity against SARS-CoV-2, with IC_{50} values of 13.84 μM and 4.63 μM (compounds III and IV, respectively), as shown in Figure 1 [29]. Moreover, the literature revealed that some isatin derivatives (methylthiazol-2(3H)-ylidene)hydrazineylidene)indolin-2-one) displayed prominent antiviral activities as HIV reverse transcriptase inhibitors, with IC_{50} values of 12.50 and 15.00 μM (compounds V and VI, respectively), as shown in Figure 1.
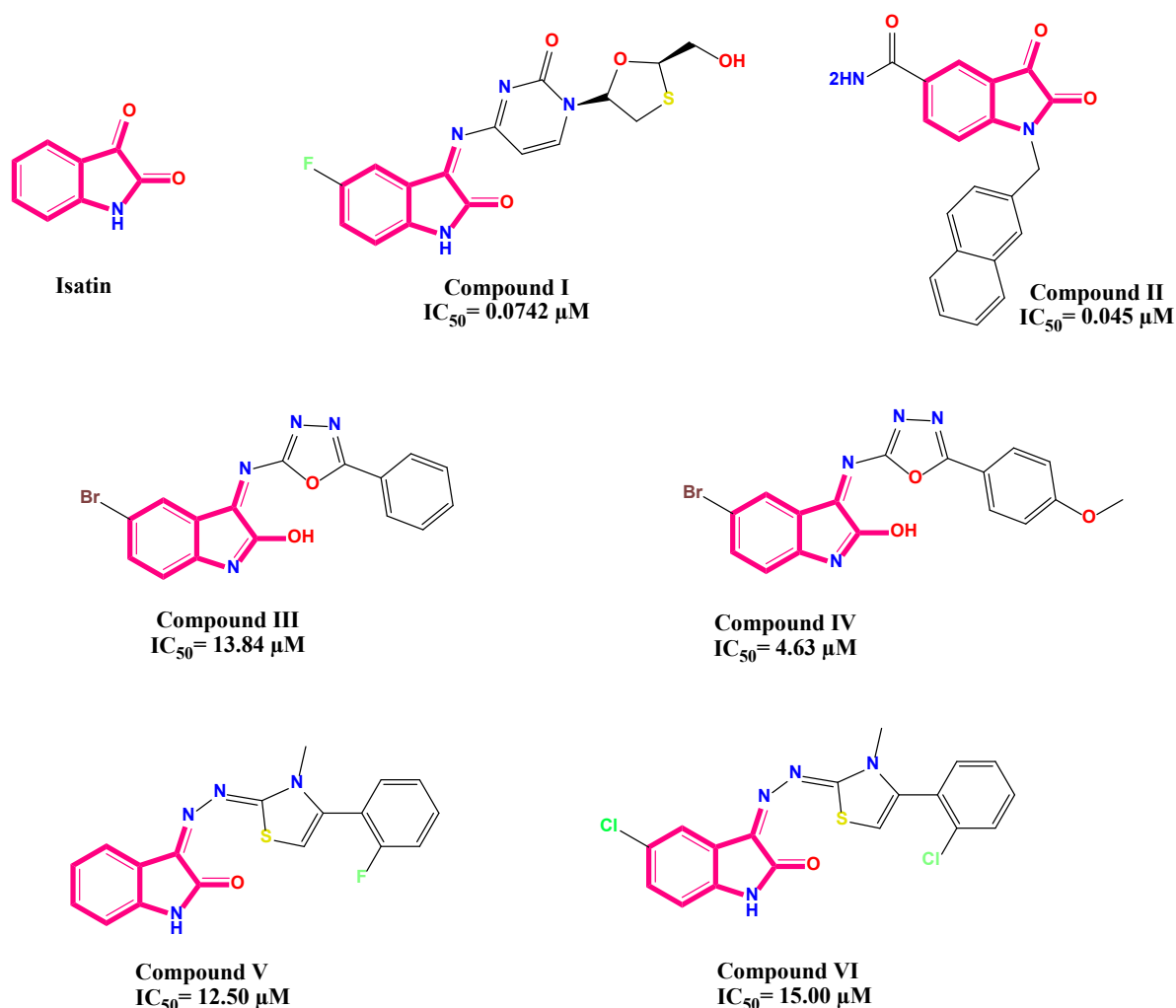
Figure 1. Some reported isatin derivatives and their corresponding IC_{50} as outstanding antiviral agents.

Comparable to remdisivir, isatin-based imidazole derivatives exhibited significant activity against SARS-CoV-2 RNA-dependent RNA polymerase (RdRp) after conducting receptor–ligand interaction studies [30]. Consequently, in this current work, our objective was to synthesize new isatin derivatives as broad-spectrum antiviral agents and assess their activities using in vitro and in silico approaches.

2. Results and Discussion

2.1. Chemistry

The synthetic pathways used for preparing the new isatin sulonylpiperidinyl derivatives in this study are depicted in Schemes 1 and 2. The starting material trifluoromethyl piperidin-1-ylsulfonyl isatin **1** was prepared via the reaction of chlorosulfonyl isatin with trifluoromethylpiperidine (achiral compound, Sigma Aldrich, St. Louis, MO, USA, CAS number: 768-31-0) according to the previously reported procedure [31].

The structures of the synthesized compounds were verified using spectrum data and elemental analyses. The ^{1}H-NMR spectrum showed a multiplet at δ 1.53 ppm, two triplets at δ 2.35 and 2.83 ppm, a doublet at δ 3.70 ppm, and a multiplet at δ 4.00 ppm, corresponding to the trifluoromethyl piperidinyl protons. Furthermore, the aromatic region displayed a singlet signal at δ 8.07 ppm attributed to the indolinone-C_4 proton and a singlet signal at δ 11.16 ppm for the NH proton, which was exchangeable with D_2O. Moreover, ^{13}C NMR displayed two signals at δ 163.09, and 179.24 ppm, assigned for two carbonyl carbons. The nucleophilic condensation of trifluoromethyl piperidin-1-ylsulfonyl isatin **1** with hydrazine hydrate afforded the hydrazono indolinone derivatives **2**. Similarly, the phenyl hydrazonoindolinone analog **3** was obtained via the condensation of starting material **1** with phenyl hydrazine. The quartet signal splitting of the trifluoromethyl group's carbon in ^{13}C NMR did not appear clearly, and this could be attributed to the low signal-to-noise ratio, the quartet splitting, and the fact that all quaternary carbons do not experience the large Overhauser enhancement provided via proton decoupling that CH carbons do.

The compound's structure was verified using spectrum data and elemental analyses. The IR spectrum of compound **2** showed three absorption bands at 3400, 3244, and 3151 cm^{-1} attributed to the NH_2 and NH functional groups. The ^{1}H-NMR spectrum showed two singlet signals at δ 10.65 and 11.14 ppm, which were exchangeable with D_2O and corresponded to the NH_2 and NH protons, respectively. The IR spectrum of compound **3** displayed two singlet signals at δ 11.43 and 12.83 exchangeable with D_2O and attributed to NH protons.

Similarly, sulfonyl indolinylidene benzohydrazide and indolinylidene benzenesulfonohydrazide analogs **4** and **5** were synthesized by condensing trifluoromethyl piperidin-1-ylsulfonyl isatin **1** with either benzoylhydrazine or benzenesulfonyl hydrazide, respectively. Their structures were confirmed using analytical and spectral data. The IR spectrum of compound **4** exhibited two absorption bands at 1710 and 1652 cm^{-1}, corresponding to the two carbonyl functional groups. The ^{1}H-NMR spectrum showed a triplet signal at δ 7.12, a doublet at δ 7.55, and another triplet at δ 7.63 ppm confirming the presence of the phenyl ring.^{13}C-NMR showed two signals at δ 160.58 and 164.60 ppm, indicating the presence of the two carbonyl carbons. Additionally, the ^{1}H-NMR spectrum of benzenesulfonyl hydrazide derivative **5** showed a triplet at δ 7.06, a doublet at δ 7.30, and a triplet at δ 7.40 ppm, indicating the phenyl ring protons. The mass spectrum of compound **5** displayed a molecular ion peak at m/z = 516. Two Schiff's bases were prepared by reacting trifluoromethyl piperidin-1-ylsulfonyl isatin **1** with two aniline derivatives in absolute ethanol containing glacial acetic acid. Thus, the 3-Arylimino isatin derivatives **6a,b** were synthesized. The mass spectrum of the chlorophenylimino indolinone **6a** displayed the M^{2+} and M^+ at m/z: 473 and 471, respectively, corresponding to the chlorine isotopes. The chemical behavior of the isatin analog **1** towards three aromatic diamino compounds was also discussed. Cyclo-condensation occurs in the case of *o*-phenylenediamine, resulting in the formation of indolo[2,3-b]quinoxaline hybrid derivative **7**. When equimolar quantities of trifluoromethylpiperidin-1-ylsulfonyl isatin **1** and *p*-phenylenediamine were heated in absolute ethanol containing acetic acid, the 3-(4-aminophenyl) iminoisatin derivative **8** was afforded. The structure of compound **7** was confirmed via elemental analysis and spectral data. ^{13}C-NMR showed two signals at δ 154.77 and 155.04 ppm attributed to the two C=N groups. Finally, 4,4′-sulfonyldianiline (Dapsone) was condensed with the starting material trifluoromethylpiperidin-1-ylsulfonyl isatin **1** to afford aminophenyl sulfonylphenyl imi-

noisatin analog **9**. The ^{1}H-NMR spectrum of compound **9** exhibited a singlet signal at δ 5.90 ppm, corresponding to NH$_2$ protons, and disappeared in D$_2$O.

2.2. Biological Evaluation

The newly synthesized compounds will be tested for their antiviral activities on influenza virus (H1N1), herpes simplex virus 1 (HSV-1), and coxsackievirus B3 (COX-B3).

2.2.1. Cytotoxicity Assay

Cytotoxicity studies are utilized to assess the safety of a drug on cells in the early stages of drug development. This approach is a useful way for identifying the toxic dose and potentially harmful effect of the tested drug. The cytotoxicity assay was performed on Vero cell lines. The synthesized compounds displayed a high cytotoxic concentration of 50 (CC$_{50}$), ensuring their safety. Notably, the least toxic one was compound **7**, with a CC$_{50}$ value of 315,578.68 µM, followed by compound **5**, with a CC$_{50}$ value of 64,451.8 µM, while the most toxic one was compound **9**, with a CC$_{50}$ value of 10 µM, as depicted in Supplementary Tables S1–S3.
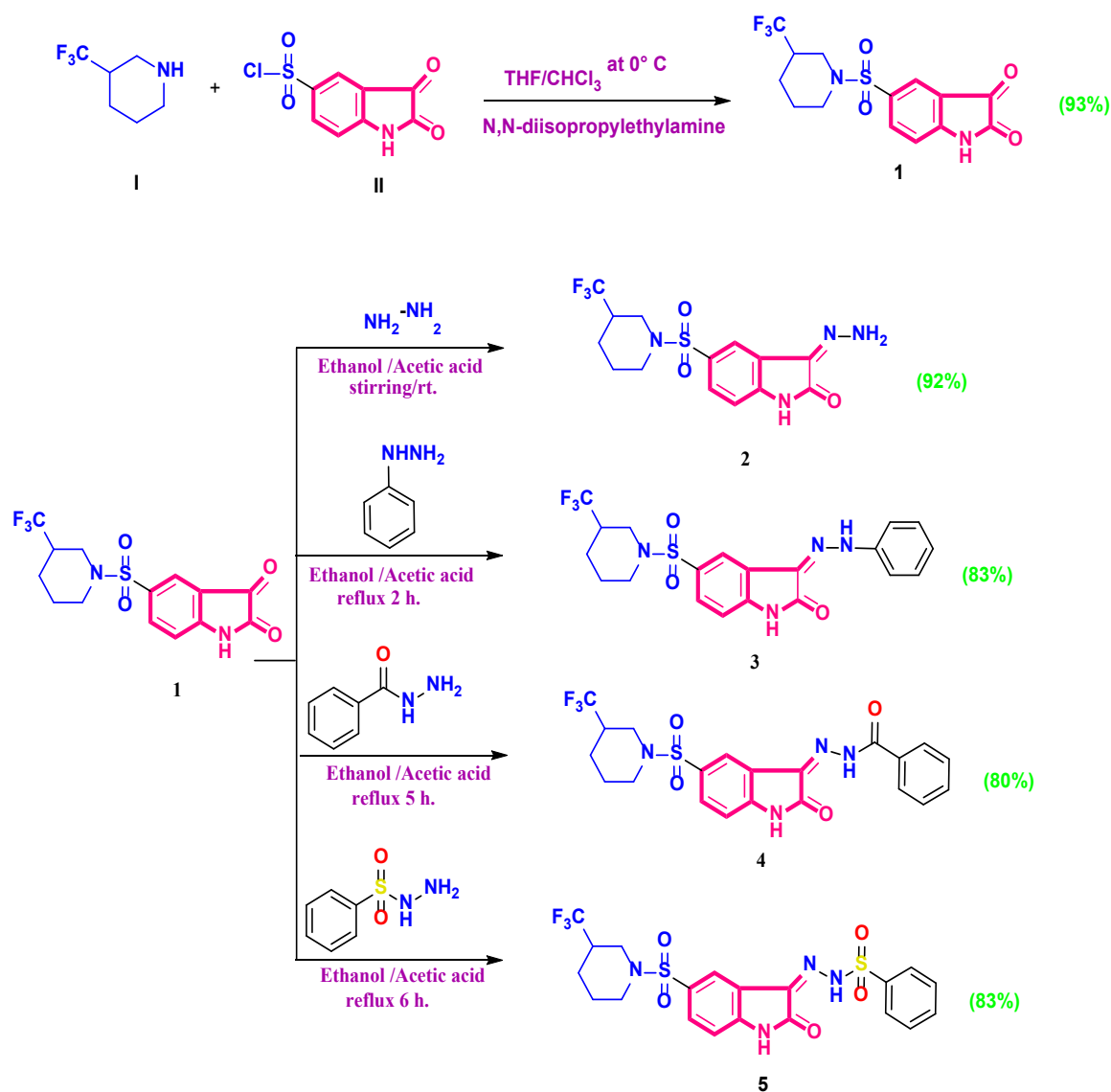
Scheme 1. The chemical synthesis of 5-((3-(trifluoromethyl)piperidin-1-yl)sulfonyl)indoline-2,3-dione derivatives (compounds **1**–**5**) as outstanding antiviral candidates.
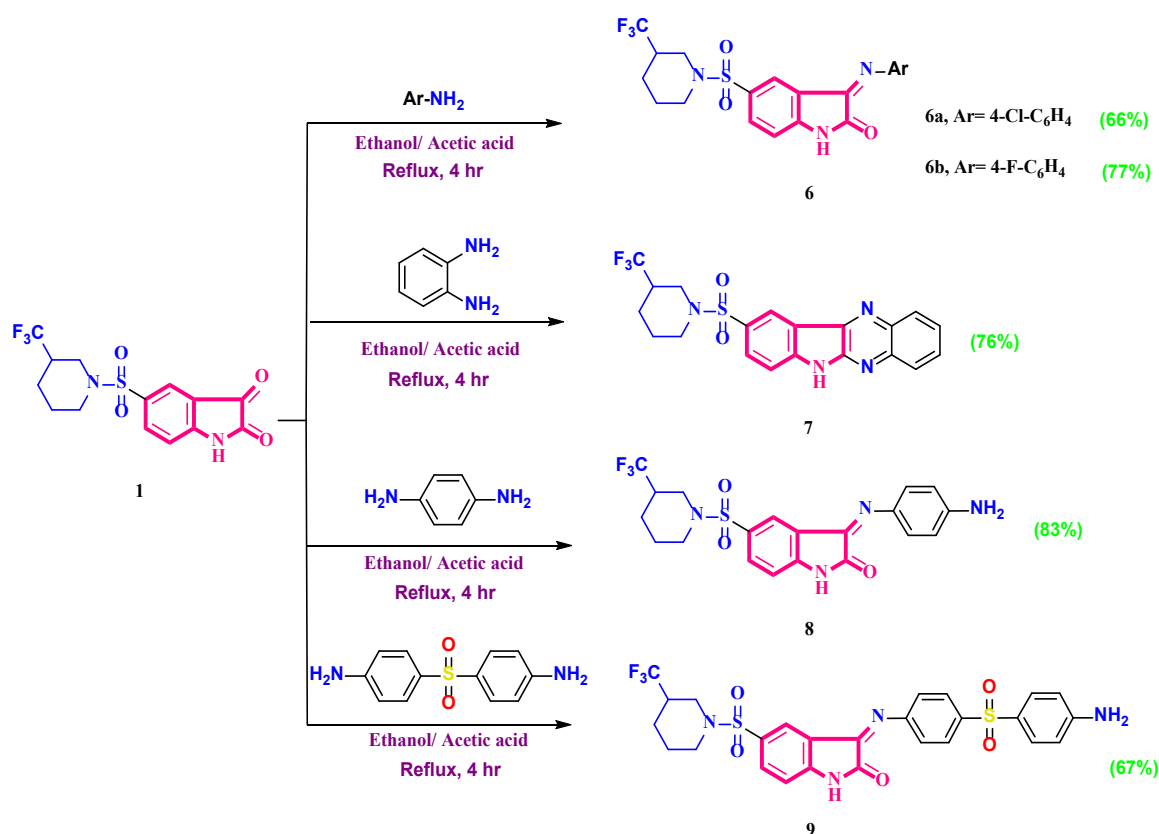
Scheme 2. The chemical synthesis of 5-((3-(trifluoromethyl)piperidin-1-yl)sulfonyl)indoline-2,3-dione derivatives (compounds **6**–**9**) as outstanding antiviral candidates.

2.2.2. The Antiviral Activity Assay (Inhibitory Concentration 50 Detection)

The synthesized compounds were tested for their antiviral activity against influenza virus H1N1 on MDCK cell lines and against HSV-1 and COX-B3 on the Vero cell lines. The synthesized compounds exhibited low inhibitory concentration 50 (IC_{50}), ensuring their eligible antiviral activities against the three investigated viruses, as illustrated in Figure 2. The different concentrations of each compound were incubated with 100 $TCID_{50}$ of each virus at an MOI of 0.1. The compounds were tested for their antiviral activity against influenza virus H1N1 on the MDCK cell line. The highest antiviral activity was displayed in compound **9**, with an IC_{50} value of 0.0027 μM, followed by compounds **6b**, **4**, and **8**, with IC_{50} values of 0.0051, 0.0087, and 0.0097 μM, respectively. However, we can consider compound **8** as the best due to its high selectivity index (3,663,901.03), as shown in Table S1. Regarding HSV-1, the most effective one was compound **5**, with an IC_{50} value of 0.0022 μM and selectivity index (SI) of 29,296,272.73, followed by compound **2**, with an IC_{50} value of 0.0035 μM and selectivity index (SI) of 112,654.29. However, compounds **3** and **4** had no activity (Table S2). When testing against COX-B3, the highest activity was exhibited in compound **4**, with an IC_{50} value of 0.0092 μM, followed by compounds **2** and **3**, with IC_{50} values of 0.0096 μM and 0.0097 μM. However, compound **3** was regarded as the best one due to its higher SI (41,071.88). On the contrary, compound **9** had no antiviral activity (Table S3).
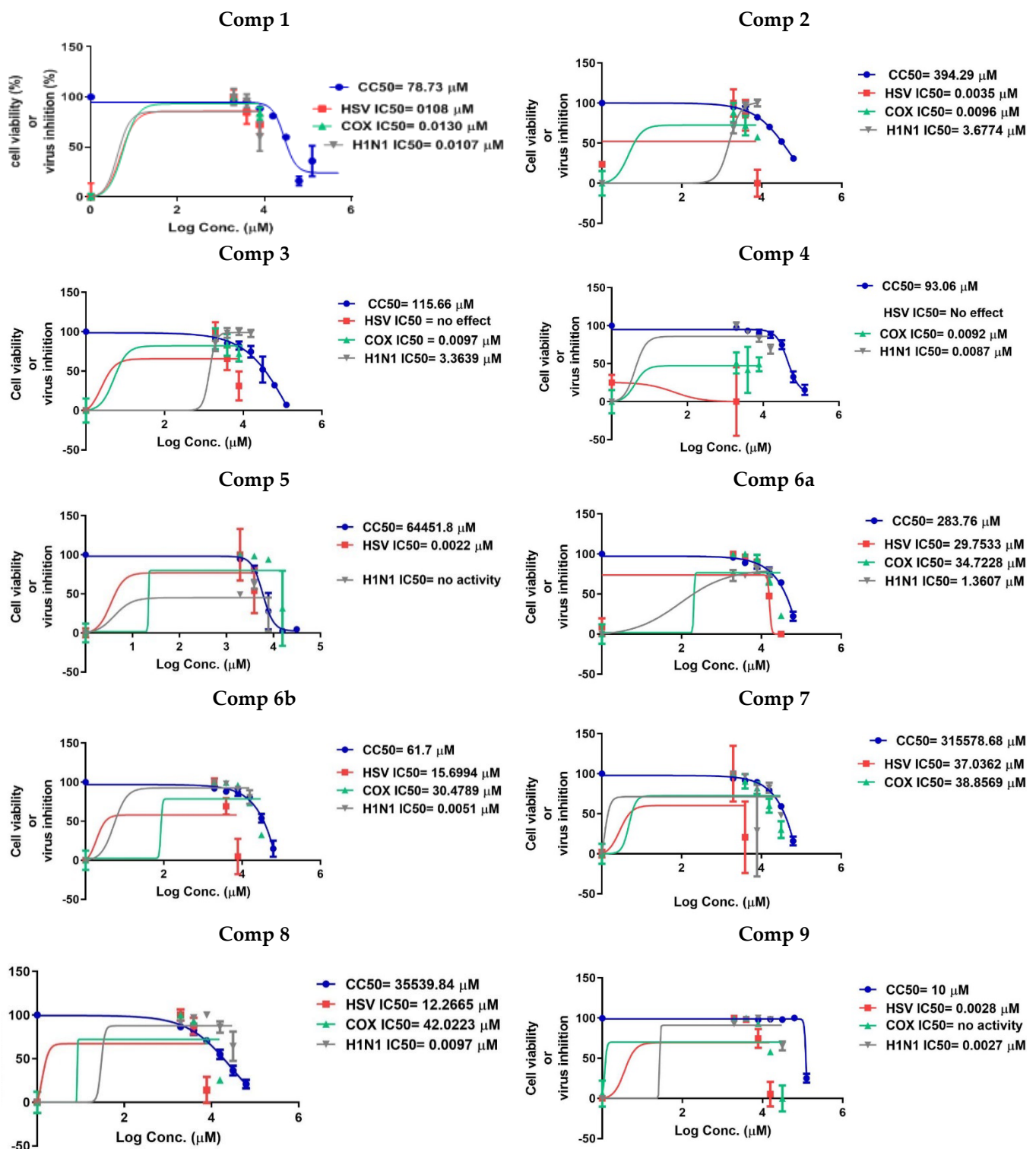
Figure 2. Cytotoxicity, anti-H1N1, anti-HSV1, and anti-COX B3 activities of studied compounds in MDCK and Vero cells. The CC_{50} and IC_{50} of different compounds were obtained via a crystal violet assay and calculated using nonlinear regression analysis of GraphPad Prism software (version 5.01) by plotting log inhibitor versus normalized response (variable slope). CC_{50} is the cytotoxic concentration, and IC_{50} is the half-maximal inhibitory concentration.

2.2.3. Quantitative PCR (qPCR) Assay

A quantitative PCR (real-time PCR) assay was carried out for the most relevant compounds exhibiting the highest antiviral effect. The selected compounds decreased the viral gene expression by different values (Table 1). For H1N1 viruses, compounds **1**, **2**, **6b**, and **6a** decreased the viral gene expression by 1.9, 1.7, 2, and 1.5, respectively, in comparison to the viral control (2.1). For HSV, compounds **1**, **2**, **6b**, and **6a** decreased viral gene expression by 1.7, 1.5, 1.7, and 1.3, respectively, in comparison to the viral control (1.9). For COX B3, compounds **1**, **2**, **6b**, and **6a** decreased viral gene expression by 1.4, 1.5, 1.5, and 1.2, respectively, in comparison to the viral control (1.7). All compounds tested using qPCR showed a decreased expression of the viral genes (showing antiviral effect). However, the most effective one among the three investigated viruses was compound **6a**. The relative gene expression levels for the assessed samples were illustrated in Supplementary Figure S1.

Table 1. Smad2/3 qPCR data analysis using double delta Ct analysis gene for the selected compounds.

	Samples	Gene Being Tested Experimental (TE) (CT)	Gene Being Tested Control (TC) (CT)	House-Keeping Gene Experimental (HE) (CT)	House-Keeping Gene Control (HC) (CT)	ΔCt Values for the Experimental (ΔCTE)	ΔCt Values for the Control (ΔCTC)	Delta Ct Value ($\Delta\Delta$Ct)	$2^{-\Delta\Delta Ct}$ (Expression Fold Change) Fold Expression Level in the Experimental Condition the Expression as in the Control Condition
H1N1	V H1N1	27	22.4	26.9	21.2	0.1	1.2	−1.1	2.1
	C H1N1	28	22.4	26.8	21.2	1.2	1.2	0	1.0
	Comp. 1	27	22.4	26.7	21.2	0.3	1.2	−0.9	1.9
	Comp. 2	27.1	22.4	26.7	21.2	0.4	1.2	−0.8	1.7
	Comp. 6b	27.1	22.4	26.9	21.2	0.2	1.2	−1	2.0
	Comp. 6a	27.3	22.4	26.7	21.2	0.6	1.2	−0.6	1.5
HSV-1	V HSV	27.4	22.6	26.7	21	0.7	1.6	−0.9	1.9
	C HSV	28	22.6	26.4	21	1.6	1.6	0	1.0
	Comp. 1	27.5	22.6	26.7	21	0.8	1.6	−0.8	1.7
	Comp. 2	27.6	22.6	26.6	21	1	1.6	−0.6	1.5
	Comp. 6b	27.4	22.6	26.6	21	0.8	1.6	−0.8	1.7
	Comp. 6a	27.7	22.6	26.5	21	1.2	1.6	−0.4	1.3
COX-B3	V COX	24.4	22	24.6	21.4	−0.2	0.6	−0.8	1.7
	C COX	25.6	22	25	21.4	0.6	0.6	0	1.0
	Comp. 1	24.8	22	24.7	21.4	0.1	0.6	−0.5	1.4
	Comp. 2	24.4	22	24.4	21.4	0	0.6	−0.6	1.5
	Comp. 6b	24.5	22	24.5	21.4	0	0.6	−0.6	1.5
	Comp. 6a	24.9	22	24.6	21.4	0.3	0.6	−0.3	1.2

V: (virus control); Cell culture lysate of cells infected with virus only, **C:** (cell control); not treated with neither virus nor compound, then cells treated with both virus and compound were taken, **CT:** Cycle threshold.

2.3. In Silico Studies

2.3.1. Molecular Docking Studies

The binding affinities of the synthesized compounds to the three studied viruses were investigated by conducting molecular docking studies. Since the literature has revealed that isatin derivatives can act on HIV reverse transcriptase [32–34], which belongs to viral polymerase enzymes, the established molecular docking was performed on the polymerases of the three investigated enzymes using the MOE docking program. Subsequently, prescreening validation was carried out to ensure MOE program accuracy and validity. The validation was performed by re-docking the co-crystallized ligand and pursuing the attained RMSD values for multiple poses. The pose with a feasible RMSD value was selected to ensure the program's validity. Thus, low RMSD values were attained, emphasizing the employed MOE program validity [35–38], as shown in Supplementary Figures S2 and S3. Consequently, the molecular docking program was run for all the synthesized compounds (**1–9**) along with the co-crystallized ligands and reference control. The docking binding scores, the binding interactions, and RMSD values at polymerase target protein of H1N1, HSV, and Coxackievirus B3 were depicted in Supplementary Table S4.

Owing to their outstanding activity against H1N1 influenza, HSV, and Coxackievirus B3, the molecular docking results of compounds **9**, **5**, and **4**, respectively, were pursued and underscored along with the corresponding co-crystallized ligands and reference control.

Regarding the H1N1 influenza virus, the docking results attained revealed that the docked co-crystallized ligand at the RNA polymerase active site exhibited a binding score of -6.11 kcal/mol with an RMSD value of 1.11 Å. Moreover, the two hydroxyl groups at positions 1 and 2 of the phenyl ring of the crystallized ligand could form hydrogen bonds with GLU65 and GLU104 at distances of 3.05 and 2.88 Å, respectively, as shown in Figure 3. However, the molecular docking results displayed that compound **9** exhibited a binding score of -7.35 kcal/mol, surpassing the binding score of the co-crystallized ligand with an RMSD value of 1.88 Å. The indolyl sulfonyl group could form hydrogen bonds with GLU180 and LYS39 at distances of 3.36 and 3.18 Å, whereas the phenyl sulfonyl group could form hydrogen bonds with LEU91 at a distance of 3.02 Å. In addition, the fluoride atom of the trifluoromethyl group could form hydrogen bonds with LYS122 at a distance of 3.21 Å, as shown in Figure 4.
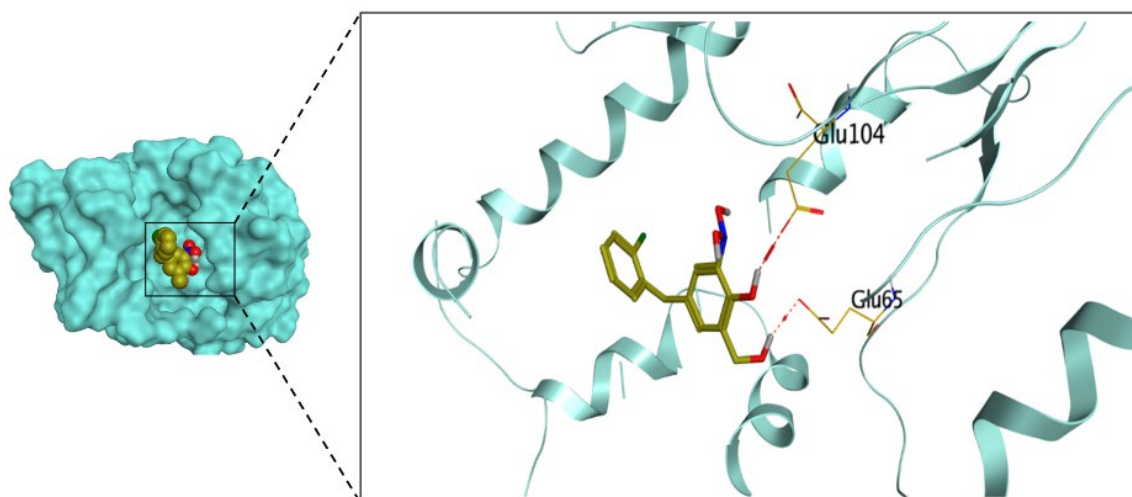

Figure 3. The 3D protein positioning and 3D binding interactions of the co-crystallized ligand at RNA polymerase active site of H1N1 Influenza virus.
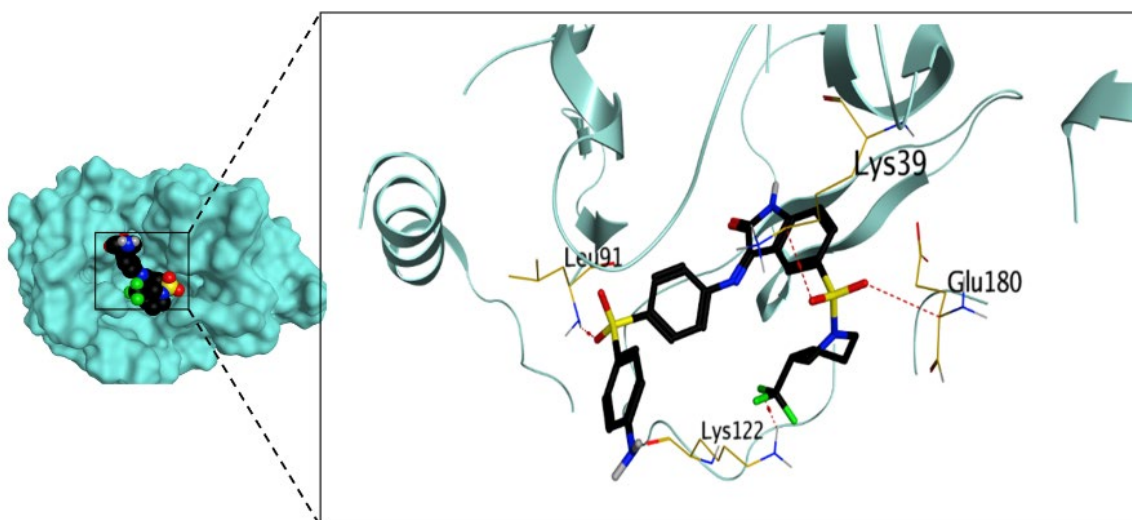

Figure 4. The 3D protein positioning and 3D binding interactions of compound **9** at RNA polymerase active site of H1N1 Influenza virus.

Regarding the HSV virus, the docking results attained revealed that the docked co-crystallized ligand at the DNA polymerase active site exhibited a binding score of −8.13 kcal/mol with an RMSD value of 1.29 Å. Moreover, the methylene bridge between the morpholine ring and quinoline moiety could form a hydrogen bond with DC1 at a distance of 3.11 Å. Moreover, the morpholine ring could form hydrogen bonds with ASP888 and ASN815 at distances of 3.14 and 2.86 Å, respectively. The oxo group at position 4 of the quinoline moiety could form a hydrogen bond with TYR818 at a distance of 2.90 Å. Additionally, the amide group of the co-crystallized ligand could form a hydrogen bond with ASN815 at a distance of 3.21 Å. Finally, the cholorphenyl moiety could form a pi-H bond with SER816 at a distance of 4.19 Å, as shown in Figure 5. However, the molecular docking results displayed that compound **5** exhibited a binding score of −6.48 kcal/mol with an RMSD value of 1.36 Å. The hydrazine moiety of compound **5** could form ASN815 3.13 Å, as shown in Figure 6.
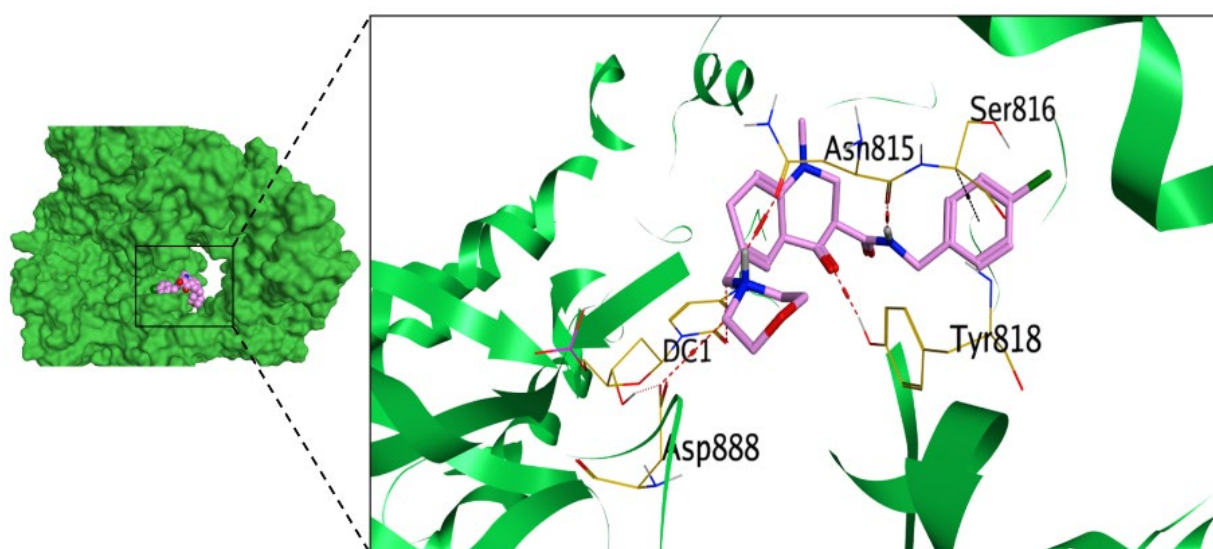

Figure 5. The 3D protein positioning and 3D binding interactions of the co-crystallized ligand at DNA polymerase active site of HSV.

Figure 6. The 3D protein positioning and 3D binding interactions of compound **5** at DNA polymerase active site of HSV.

Regarding Coxackievirus B3, the docking results attained revealed that the reference control compound at the RNA polymerase selected site exhibited a binding score of −5.70 kcal/mol with an RMSD value of 1.75 Å. Moreover, the pyrazine moiety of the reference compound could form a pi-H bond with ARG174 at a distance of 3.52 Å. In addition, the guanidine moiety could form hydrogen bonds with ARG174, ASP329, and TYR234 at distances of 3.06, 2.95, and 3.17 Å, respectively, as displayed in Figure 7. On the other hand, the molecular docking results displayed that compound **4** exhibited a binding score of −7.41 kcal/mol, surpassing the binding score of the reference drug with an RMSD value of 1.46 Å. The sulfonyl group of compound **4** could form a hydrogen bond with ASP238 at a distance of 3.08 Å. Additionally, the oxo group of the isatin moiety of compound **4** could form a hydrogen bond with LYS376 at a distance of 2.98 Å, as shown in Figure 8. The 2D/3D binding interactions and 3D protein positioning of all the synthesized compounds along with the co-crystallized ligand and reference control were depicted in Supplementary Table S5.

Figure 7. The 3D protein positioning and 3D binding interactions of the reference drug at RNA polymerase selected site of Coxackievirus B3.
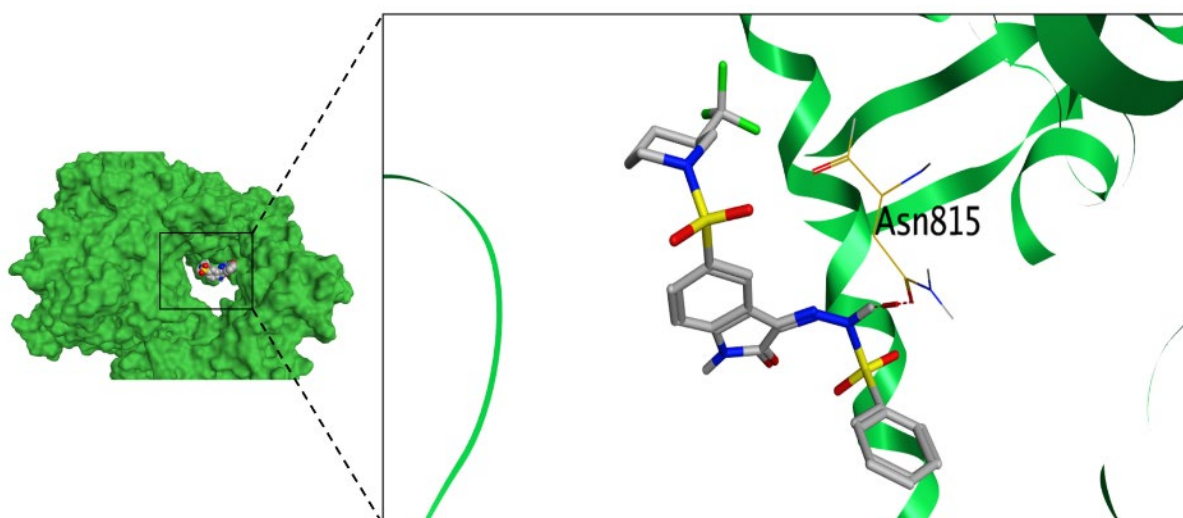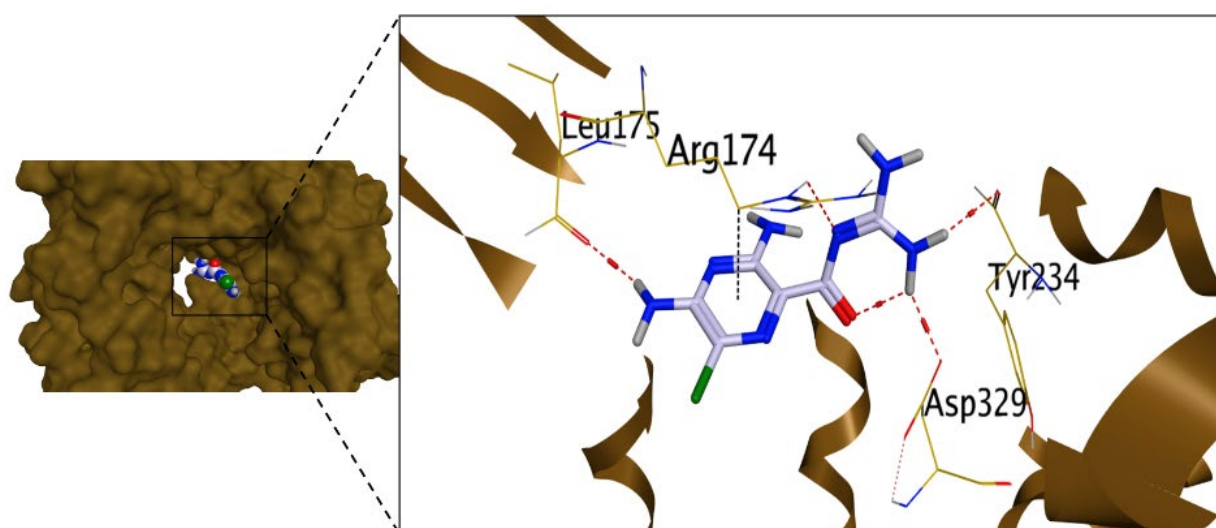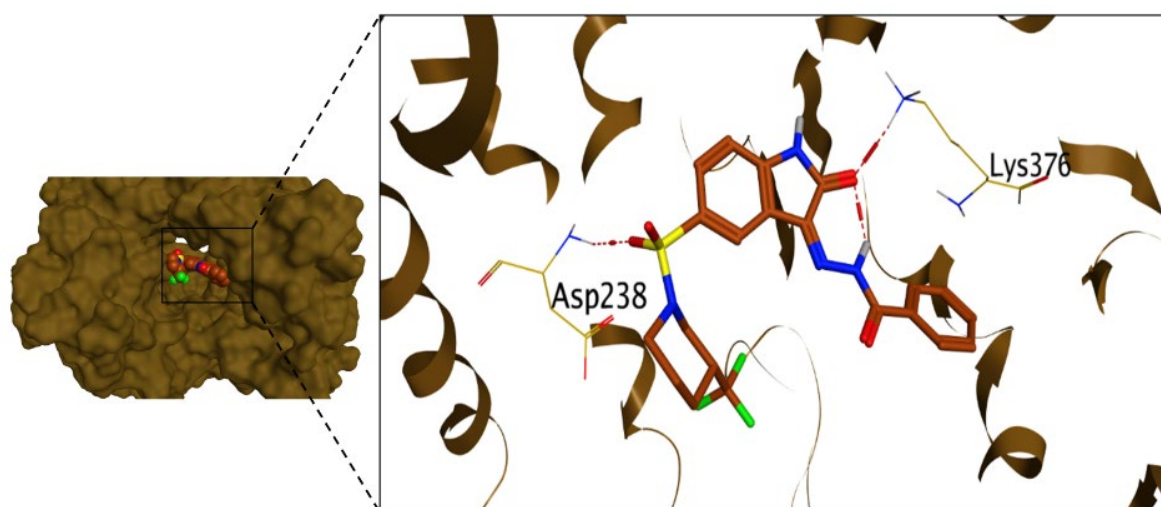

Figure 8. The 3D protein positioning and 3D binding interactions of compound **4** at RNA polymerase selected site of Coxackievirus B3.

2.3.2. In Silico ADME Predictions

Bioavailability and pharmacokinetics are becoming more important in the in silico prediction of molecular physicochemical properties to examine potential drug compounds as a result of drug development [39,40]. Theoretical studies are crucial in this area for quickly and easily obtaining reliable data. Recently, a number of free online interfaces have been established for rapid screening and reducing costs for drug candidate studies (without requiring animal testing) [41]. SwissADME is a brand-new, in-depth tool developed by the Swiss Institute of Bioinformatics (SIB) that simplifies the assessment of ADME parameters for medication candidates, such as absorption, distribution, metabolism, and excretion. Initially, in the process of creating a medication, ADME characteristics [42] are crucial in determining whether a medicine will likely reach its target or be removed from the organism. Based on the observed physicochemical norms, these criteria can be validated via computational in silico investigations. The latter emphasizes molecular size, flexibility, polarity, saturation, or water solubility [43]. Another way to consider drug likeness is as a delicate balance between chemical and structural traits that determine whether the molecule under study is similar to recognized medications. The "Rules of 5" (RO5), commonly known as Lipinski's rules or Pfizer's rules, was established by Christopher Lipinski in 1997. It evaluates drug likeness based on a variety of parameters, including molar mass (500 g/mol), log P (5), the number of H-bond acceptors (10; for atoms of nitrogen or oxygen of chemical compound), and the number of H-bond donors (5; for molecular characteristics pertaining to OH or NH groups). In addition to Ghose's contribution [44], the guidelines of Veber [45], Egan [46,47], and Muegge [48] are also used to predict drug likeness. Additionally, SwissADME includes "BOILED-egg evaluation" [49–53], which provides insights into human gastric absorption and the blood–brain barrier (BBB) (HIA). An in silico evaluation of the recently synthesized compounds 1, **2**, **3**, **4**, **5**, **6a**, **6b**, **7**, **8,** and **9** was carried out utilizing the SwissADME web tool for drug likeness prediction, physical and chemical properties, solubility, lipophilicity, pharmacokinetics, and medicinal chemistry. Tables 2 and 3 present an overview of the findings. The compounds under investigation exhibit ADME-friendly characteristics. Each compound also adheres to the ideal Lipinski law principles, which denotes drug likeness. In addition to their good absorption (ABS), each compound has a bioavailability score of 0.55, ensuring good pharmacokinetic features. The percentage of ABS, a specialized physiochemical parameter, influences the characteristics of drug transport using the equation of %ABS = 109 − (0.345 × TPSA) [54,55]. The synthesized compounds 1, **2**, **3**, **4**, **6a**, **6b**, **7**, and **8** with values of TPSA < 140 A^2 represent the considerable permeability of the cellular plasma membrane falling below 140 A^2, indicating substantial permeability in the cellular plasma membrane. All synthesized compounds demonstrated high gastrointestinal (GI) absorption, except for compounds **5** and **9,** as depicted in Figure 9. Furthermore, the molar refractivity values (ranging from 84.17 to 148.82) were within the acceptable range. The synthetic compounds display fairly good values of skin permeability, ranging from moderate to good (log Kp; where Kp in cm/s; with $-8.73 <$ log Kp < -7.11) [56]. Moreover, log S (ESOL criteria) indicates good solubility in the body [57]. While SILICOS-IT used a fragment-dependent method for Log S estimates, the methods of Ali and others rely on the full molecular topology. Bioavailability radars for the compounds examined could be subjected to intuitive analysis (Figure S4). These unique snapshots for SwissADME are drug similarity graphs, which are expressed in a hexagonal shape, with each vertex displaying a parameter that reflects a product's bioavailability. The ideal range of numerous parameters, such as lipophilicity, can be seen in the pink regions (XLOGP3 from 0.70 to 2.80), size (molecular weight of 362–592 g/mol), and polarity (TPSA 87.22–155.76 Å^2). The red deformed hexagon in pink illustrates the characteristics of a drug. It was noted that due to the inconsistency in saturation, all compounds are just barely outside the pink area on one side. Moreover, the Egan BOILED-Egg visual categorization model (Brain or IntestinaL EstimateD) predictive model permeation diagram anticipated the in vivo ADME features. (Figure 9), including the penetration of the blood–brain barrier (BBB) and passive human gastrointestinal absorption (HIA). Finally, compounds **1**, **2**, **3**,

4, **6b**, **7**, and **8** (in the white region) exert high HIA. P-glycoprotein, represented as red dots, indicates molecules as non-substrates for P-gp (PGP-), and all the tested compounds showed non-P-gp substrate characteristics. The radar plots of the investigated compounds are shown in Supplementary Figure S4.

Table 2. Listed physicochemical and pharmacokinetic characteristics of studied compounds (**1**–**9**).

Comp. No.	iLog P	Molar Refractivity	Log S	WLOGP	TPSA (Å²)	% ABS	GI Absorption	P-gp Substrate	Log Kp
1	1.56	84.17	MS	3.17	91.93	77.28	High	No	−7.29
2	1.64	90.14	S	2.65	113.24	69.93	High	Yes	−7.03
3	1.95	116.26	PS	4.62	99.25	74.75	High	Yes	−6.31
4	1.90	119.95	PS	4.12	116.32	68.86	High	Yes	−6.59
5	1.84	122.85	PS	4.75	141.77	60.08	Low	No	−7.03
6a	2.88	117.49	PS	5.76	87.22	78.90	High	No	−6.20
6b	2.12	112.44	PS	5.67	87.22	78.90	High	Yes	−6.48
7	2.78	110.92	PS	6.19	87.33	78.87	High	Yes	−6.04
8	2.18	116.89	PS	4.70	113.24	69.93	High	Yes	−7.02
9	2.61	148.82	PS	6.62	155.76	55.26	Low	No	−7.30

iLog P: lipophilicity, **Log S**: water solubility (SILICOS-IT; S-soluble, MS: moderately soluble, PS: poorly soluble), **TPSA**: topological polar surface area [Å²]. **In silico % absorption** (%ABS) = $109 - (0.345 \times TPSA)$. **GI-absorption**: gastrointestinal absorption. **P-gp**: p-glycoprotein inhibitors. **Log Kp**: skin permeability coefficient (Kp in cm/s).

Table 3. Expectations of drug likeness for tested compounds (**1**–**9**).

| Comp. No	Mol. Weight [g/mol]	Lipophilicity (MLogP)	H-Bond Donors	H-Bond Acceptors	Lipinski Violations	Ghose Viol.	Veber Viol.	Egan Viol.	Muegge Viol.	Bioavailability Score
1	362.32	0.70	1	8	Yes; 0	Yes	Yes	Yes	Yes	0.55
2	376.35	0.72	2	8	Yes; 0	Yes	Yes	Yes	Yes	0.55
3	452.45	2.15	2	8	Yes; 0	Yes	Yes	Yes	Yes	0.55
4	480.46	1.92	2	9	Yes; 0	No; 1	Yes	Yes	Yes	0.55
5	516.51	1.26	2	10	Yes; 1	No; 1	No; 1	No; 1	Yes	0.55
6a	471.88	2.63	1	8	Yes; 0	No; 1	Yes	Yes	Yes	0.55
6b	455.43	2.52	1	9	Yes; 0	No; 1	Yes	Yes	Yes	0.55
7	434.43	2.80	1	8	Yes; 0	No; 1	Yes	No; 1	Yes	0.55
8	452.45	1.61	2	8	Yes; 0	Yes	Yes	Yes	Yes	0.55
9	592.61	2.29	2	10	Yes; 1	No; 3	No; 1	No; 2	No; 1	0.55
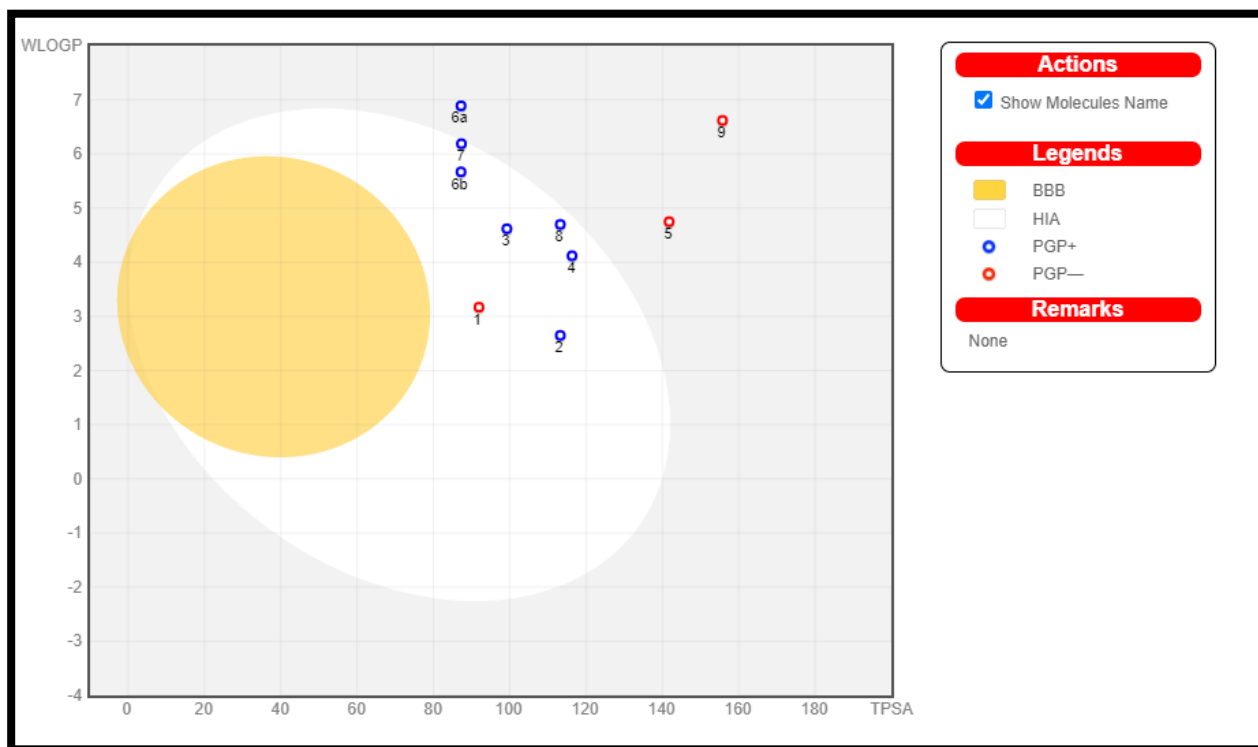
Figure 9. Expected BOILED-Egg diagram for the investigated compounds (**1**–**9**) using Swiss ADME web tool, where the egg white represents high GIT absorption, and the egg yolk represents the blood–brain barrier passing.

2.4. Structure–Antiviral Activity Relationship

A structure–antiviral activity relationship (SAR) study was carried out so that we can gain a far deeper understanding of the antiviral activity changes upon future structural modification. The conducted SAR was performed based on the antiviral activity (IC$_{50}$ values) of the synthesized isatin derivatives against the three investigated viruses.

Considering the influenza H1N1 virus, it was revealed that the best activity was attained when the isatin scaffold was substituted with 4,4′-sulfonyldianiline (compound **9**). Moreover, satisfactory antiviral activity was attained by substituting the isatin scaffold with 4-fluoroaniline, benzohydrazide, and benzene-1,4-diamine (compounds **6b**, **4**, and **8**, respectively). However, the least antiviral activity was displayed by substituting the isatin scaffold with benzenesulfonohydrazide (compound **5**), as shown in Figure 10.

On the other hand, regarding HSV, it was revealed that the best activity was attained when the isatin scaffold was substituted with benzenesulfonohydrazide (compound **5**). Additionally, worthy antiviral activity was attained by substituting the isatin scaffold with 4,4′-sulfonyldianiline (compound **9**) and hydrazine (compound **2**). However, the least antiviral activity was exhibited by substituting the isatin scaffold with phenylhydrazine (compound **3**) and benzohydrazide (compound **4**), as depicted in Figure 10.

Furthermore, considering Coxackievirus B3, it was shown that the best activity was attained when the isatin scaffold was substituted with benzohydrazide (compound **4**). In addition, eligible antiviral activity was attained by substituting the isatin scaffold with hydrazine (compound **2**) and phenylhydrazine (compound **3**). However, the least antiviral activity was displayed by substituting the isatin scaffold with 4,4′-sulfonyldianiline (compound **9**), as illustrated in Figure 10.
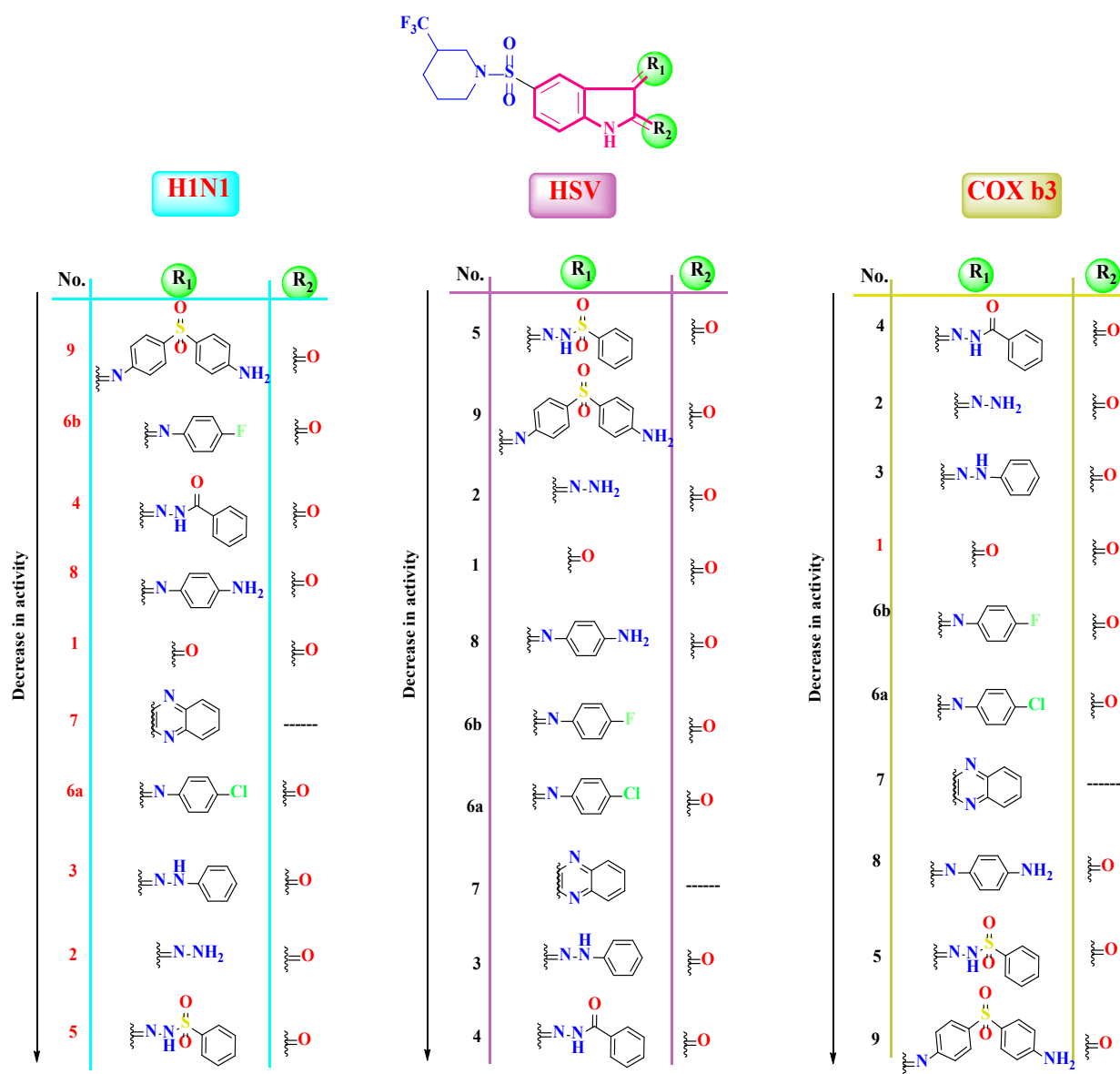
Figure 10. Structure–activity relationship of the synthesized compounds (**1**–**9**) regarding influenza H1N1, HSV, and Coxackievirus B3.

3. Conclusions

Owing to their eligible antiviral activities, as evident from the literature, the synthesized isatin derivatives (**1**–**9**) pledged promising antiviral potential against H1N1, HSV-1, and COX-B3 with remarkably low micro-molar IC_{50} values, particularly for compounds **9**, **5**, and **4**, respectively. Moreover, reliable safety on normal cells can be encountered in the synthesized compounds, particularly for compounds **7**, **5**, and **9**, owing to their significantly higher CC_{50} values. Moreover, the conducted qPCR and the decreased viral gene expression confirmed the antiviral potential claim of the synthesized compounds. Furthermore, the in silico molecular docking and ADME prediction let us gain further insights and a far deeper understanding of the binding affinities of the synthesized compounds and their reliable pharmacokinetic properties.

4. Materials and Methods

4.1. Chemistry

Reagents and solvents were attained by commercial chemical suppliers and were used without further purification. The chemicals used were supplied by Merck and Aldrich, and the reported yields refer to purified products. Thin-layer chromatography (TLC) with 0.25 mm thick Merck Silica Gel 60 F_{254} was used to check all chemical reactions established, and a UV lamp was used for visualization. Melting points were measured using Stuart SMP3 apparatus utilizing open capillary tubes. IR spectra (KBr) were recorded using Shimadzu FT/IR 1650 spectrometer (Perkin Elmer, Waltham, MA, USA). A Bruker Advance-400 instrument was used for ^{1}H and ^{13}C NMR spectra determination (400 MHz and 100 MHz were used for ^{1}H and ^{13}C, respectively) in DMSO-d_6 and are recorded in ppm values relative to TMS as an internal reference standard or to solvent used for spectrum determination. Mass spectrometry was conducted using a Shimadzu GS/MS-QP 2010 plus spectrometer at 70 eV. Biological activities were performed at Faculty of Medicine, Al-azhar University, Cairo, Egypt. The full spectral data for all the synthesized compounds were depicted in Supplementary Data S1.

5-(3-(Trifluoromethyl)piperidin-1-ylsulfonyl)isatin (1)

A solution of 5-Chlorosulfonylisatin (0.01 mmol) in 24 mL of 1:1 THF/CHCl$_3$ at 0 °C was added dropwise, via syringe pump, to a solution of trifuoromethylpiperidine (0.01 mmol) and *N*,*N*-diisopropylethylamine (0.01 mmol) in 4 mL of CHCl$_3$. The reaction was followed by TLC until complete (about 20 min). The solid was then recrystallized from EtOAc/Hexanes to give the title compound.

Yellow crystal; Yield: (93%); m.p.:249–251 °C. IR: υ/cm^{-1} = 3298 (NH), 3075, 3020 (CH-arom.), 2947, 2862 (CH-aliph.), 1765, 1744 (2C=O), 1384 (S=O).^{1}H NMR: δ/ppm = 1.53 (m, 2H, piperidinyl-CH$_2$), 2.35 (t, 2H, *J* = 4Hz, piperidinyl-CH$_2$), 2.83 (t, 2H, *J* = 4 Hz, *N*-CH$_2$), 3.70 (d, 2H, *J* = 4 Hz, *N*-CH$_2$), 4.00 (m,1H, piperidinyl-CH), 7.40 (d, 1H, *J* = 8 Hz, indolinone-C$_7$-H), 8.07 (s, 1H, indolinone-C$_4$-H), 8.48 (d, 1H, *J* = 8 Hz, indolinone-C$_6$-H), 11.16 (s, 1H, NH exchangeable with D$_2$O).^{13}C NMR: δ/ppm = 23.28, 25.10, 38.21, 47.35, 48.83 (piperidinyl-C), 111.61, 116.40, 129.56, 130.97, 136.09, 139.40 (Ar-C&CF$_3$), 145.94 (C=N), 163.09, 179.24 (2C=O). Mass spectrum exhibited a molecular ion peak at *m*/*z*: 362 (M$^+$, 29.64%) with a base peak at *m*/*z*: 150. Anal. Calc. for C$_{14}$H$_{13}$F$_3$N$_2$O$_4$S (362.32): C, 46.41; H, 3.62; N, 7.73. Found: C, 46.42; H, 3.61; N, 7.72.

3-Hydrazono-5-(3-(trifluoromethyl)piperidin-1-ylsulfonyl)indolin-2-one (2)

An equimolar amount of compound 1 (0.01 mol) and an appropriate amount of hydrazine hydrate (0.01 mol) were dissolved in ethanol containing acetic acid. The mixture was stirred at room temperature for 4 h. The filtered product was dried and crystallized from methanol.

Yellowish powder; Yield: (92%); m.p.: 209–211 °C. IR: υ/cm^{-1} = 3400, 3244, 3151 (NH$_2$ &NH), 3090 (CH-arom.), 2935, 2854 (CH-aliph.), 1709 (C=O), 1615 (C=N), 1315 (S=O). ^{1}H NMR: δ/ppm = 1.51 (m, 2H, piperidinyl-CH$_2$), 2.49 (t, 2H, *J* = 4 Hz, piperidinyl-CH$_2$), 2.83 (t, 2H, *J* = 4 Hz, *N*-CH$_2$), 3.72 (d, 2H, *J* = 4 Hz, *N*-CH$_2$), 4.25 (m 1H, piperidinyl-CH), 7.04 (d, 1H, *J* = 8 Hz, indolinone-C$_7$-H), 8.04 (s, 1H, indolinone-C$_4$-H), 8.18 (d, 1H, *J* = 8 Hz, indolinone-C$_6$-H), 10.65, 11.14 (2s, 3H, NH&NH$_2$ exchangeable with D$_2$O). ^{13}C NMR: δ/ppm =23.25, 26.16, 38.92, 47.34, 48.45 (piperidinyl-C), 114.59, 117.50, 120.74, 126.96, 132.79, 135.38 (Ar-C&CF$_3$), 142.31 (C=N), 162.40 (C=O). Mass spectrum exhibited a molecular ion peak at *m*/*z*: 376 (M$^+$, 39.64%) with a base peak at *m*/*z*: 219. Anal. Calc. for C$_{14}$H$_{15}$F$_3$N$_4$O$_3$S (376.08): C, 44.68; H, 4.02; N, 14.89. Found: C, 44.67; H, 4.01; N, 14.91.

3-(2-Phenylhydrazono)-5-(3-(trifluoromethyl)piperidin-1-ylsulfonyl)indolin-2-one (3)

Acetic acid (5 mL) was added to a solution of compound 1 (0.01 mol) phenylhydrazine (0.01 mol) in ethanol (20 mL), and the mixture was heated under reflux for 3 h. The resultant product was filtered, washed numerous times with small amounts of cold water, and dried. Crystallization from methanol was used to purify the chemical.

Dark red powder; Yield: (83%); m.p.: 229–231 °C. IR: υ/cm^{-1} = 3497 (br.2NH), 3060 (CH-arom.), 2921, 2884 (CH-aliph.), 1667 (C=O), 1612 (C=N), 1323 (S=O). ^{1}H NMR: δ/ppm = 1.34 (m, 2H, piperidinyl-CH$_2$), 2.30 (t, 2H, J = 4 Hz, piperidinyl-CH$_2$), 2.88 (t, 2H, J = 4 Hz, N-CH$_2$), 3.43 (d, 2H, J = 4 Hz, N-CH$_2$), 4.25 (m, 1H, piperidinyl-CH), 6.72 (t, 1H, J = 8 Hz, Ar-H), 7.36 (d, 2H, J = 8 Hz, Ar-H), 7.51(t, 2H, J = 8 Hz, Ar-H), 7.64 (d, 1H, J = 8 Hz, indolinone-C$_7$-H), 7.98 (s, 1H, indolinone-C$_4$-H), 8.43(d, 1H, J = 8 Hz, indolinone-C$_6$-H), 11.43, 12.83 (2s, 2H, two NH exchangeable with D$_2$O). ^{13}C NMR: δ/ppm =23.25, 25.45, 35.30, 42.94, 47.34 (piperidinyl-C), 110.89, 114.91, 117.82, 122.23, 124.04, 126.96, 127.74, 128.45, 129.87, 136.09, 138.30 (Ar-C&CF$_3$), 142.71 (C=N), 163.11 (C=O). Mass spectrum exhibited a molecular ion peak at m/z: 452 (M$^+$, 20.04%) with a base peak at m/z: 305. Anal. Calc. for C$_{20}$H$_{19}$F$_3$N$_4$O$_3$S (452.45): C, 53.09; H, 4.23; N, 12.38. Found: C, 53.08; H, 4.25; N, 12.37.

N′-(2-oxo-5-(3-(trifluoromethyl)piperidin-1-ylsulfonyl)indolin-3-ylidene)benzohydrazide (4)

Acetic acid (5 mL) was added to a combination of compound 1 (0.01 mol) and benzo-hydrazide (0.01 mol) in ethanol (10 mL), and the mixture was then heated under reflux for 5 h. After cooling and being treated with ice-cold water, the resultant product was filtered, dried, and crystallized from the ethanol.

Dark orange powder; Yield: (80%); m.p.: 307–309 °C. IR: υ/cm^{-1} = 3458, 3224 (2NH), 3023 (CH-arom.), 2931, 2840 (CH-aliph.), 1710, 1652 (2C=O), 1621 (C=N), 1331(S=O). ^{1}H NMR: δ/ppm = 1.48 (m, 2H, piperidinyl-CH$_2$), 2.48 (t, 2H, J = 4 Hz, piperidinyl-CH$_2$), 3.01 (t, 2H, J = 4 Hz, N-CH$_2$), 3.40 (d, 2H, J = 4 Hz, N-CH$_2$), 4.51 (m, 1H, piperidinyl-CH), 7.12 (t, 1H, J = 8 Hz, Ar-H), 7.55 (d, 2H, J = 8 Hz, Ar-H), 7.63 (t, 2H, J = 8 Hz, Ar-H), 7.72 (d, 1H, J = 8 Hz, indolinone-C$_7$-H), 7.78 (s, 1H, indolinone-C$_4$-H), 8.41(d, 1H, J = 8 Hz, indolinone-C$_6$-H), 11.35, 12.06 (2s, 2H, two NH exchangeable with D$_2$O). ^{13}C NMR: δ/ppm = 23.26, 25.09, 30.89, 46.96, 49.87 (piperidinyl-C), 111.61, 116.011, 117.12, 121.83, 128.06, 128.46, 129.87, 132.79, 133.89, 138.39, 139.79 (Ar-C&CF$_3$), 143.02 (C=N), 160.58, 164.60 (C=O). Mass spectrum exhibited a molecular ion peak at m/z: 480 (M$^+$, 19.04%) with a base peak at m/z: 70. Anal. Calc. for C$_{21}$H$_{19}$F$_3$N$_4$O$_4$S (480.46): C, 52.50; H, 3.99; N, 11.66. Found: C, 52.52; H, 3.98; N, 11.67.

N′-(2-oxo-5-(3-(trifluoromethyl)piperidin-1-ylsulfonyl)indolin ylidene) benzenesulfonohy drazide (5)

Furthermore, compound 1 (0.01 mol), benzensulfonyl hydrazine (0.01 mol), ethanol (10 mL), and acetic acid (5 mL) were combined to form a solution. The mixture was heated at reflux for six hours, cooled, and treated with ice-cold water. The resulting product was then filtered and separated from the methanol.

Reddish brown powder; Yield: (83%); m.p.: 206–208 °C. IR: υ/cm^{-1} = 3400, 3370 (2NH), 3010 (CH-arom.), 2943, 2854 (CH-aliph.), 1736 (C=O), 1623 (C=N), 1349 (S=O). ^{1}H NMR: δ/ppm = 1.52 (m, 2H, piperidinyl-CH$_2$), 1.83 (t, 2H, J = 4 Hz, piperidinyl-CH$_2$), 2.86 (t, 2H, J = 4 Hz, N-CH$_2$), 3.25 (d, 2H, J = 4 Hz, N-CH$_2$), 3.83 (m, 1H, piperidinyl-CH), 7.06 (t, 1H, J = 8 Hz, Ar-H), 7.30 (d, 2H, J = 8 Hz, Ar-H), 7.40 (t, 2H, J = 8 Hz, Ar-H), 7.52 (d, 1H, J = 8 Hz, indolinone-C$_7$-H), 7.59 (s, 1H, indolinone-C$_4$-H), 8.35 (d, 1H, J = 8 Hz, indolinone-C$_6$-H), 10.72, 11.11 (2s, 2H, two NH exchangeable with D$_2$O). ^{13}C NMR: δ/ppm = 23.57, 25.06, 37.11, 42.22, 50.97 (piperidinyl-C), 111.28, 114.61, 120.74, 120.74, 122.94, 125.15, 125.54, 128.76, 129.87, 132.08, 134.28, 136.09, 138.69, 140.90, (Ar-C&CF$_3$), 149.63 (C=N), 162.79, (C=O). Mass spectrum exhibited a molecular ion peak at m/z: 516 (M$^{\cdot+}$, 40.04%) with a base peak at m/z:86. Anal. Calc. for C$_{20}$H$_{19}$F$_3$N$_4$O$_5$S$_2$ (516.07): C, 46.51; H, 3.71; N, 10.85. Found: C, 46.50; H, 3.70; N, 10.87.

3-(Arylimino)-5-(piperidin-1-ylsulfonyl)indolin-2-one (6)

A mixture of compound 1 (0.01 mol), the required amino derivatives (0.01 mol), and ethanol (20 mL) with acetic acid (5 mL) were heated under reflux for 4 h, after which the reaction liquid was cooled to room temperature and poured over crushed ice. The product that had separated after around half an hour was filtered and washed numerous times with small amounts of cold water, dried, and crystallized from the ethanol.

3-((4-Chlorophenyl)imino)-5-((3-(trifluoromethyl)piperidin-1-yl)sulfonyl)indolin-2-one (6a)

Brown powder; Yield: (66%); m.p.: 222–224 °C. IR: υ/cm^{-1} = 3266 (NH), 3107 (CH-arom.), 2933, 2857 (CH-aliph.), 1652 (C=O), 1616 (C=N), 1330 (S=O). ^{1}H NMR: δ/ppm = 1.23 (m, 2H, piperidinyl-CH$_2$), 2.49 (t, 2H, J = 4 Hz, piperidinyl-CH$_2$), 2.86 (t, 2H, J = 4 Hz, N-CH$_2$), 3.34 (d, 2H, J = 5Hz, N-CH$_2$), 4.38 (m, 2H, piperidinyl-CH), 6.50 (d, 2H, J = 8 Hz, Ar-H), 7.01 (d, 2H, J = 8 Hz, Ar-H), 7.15 (d, 1H, J = 8 Hz, indolinone-C$_7$-H), 7.73 (s, 1H, indolinone-C$_4$-H), 8.18 (d, 1H, J = 8 Hz, indolinone-C$_6$-H), 11.45(s, 1H, NH exchangeable with D$_2$O).^{13}C NMR: δ/ppm = 18.37, 23.25, 24.98, 47.19, 49.62 (piperidinyl-C), 105.23, 111.84, 113.17, 114.61, 118.06, 121.20, 126.71, 129.48, 144.44, 145.85 (Ar-C&CF$_3$), 159.71 (C=N), 162.47 (C=O). Mass spectrum exhibited a molecular ion peak at m/z: 473 (M^{2+}, 21.78%), 471 (M$^+$, 12.22%) with a base peak at m/z: 367. Anal.Calc. for C$_{20}$H$_{17}$ClF$_3$N$_3$O$_3$S (471.88): C, 50.91; H, 3.63; N, 8.91. Found: C, 50.61; H, 3.65; N, 9.01.

3-((4-Fluorophenyl)imino)-5-((3-(trifluoromethyl)piperidin-1-yl)sulfonyl)indolin-2-one (6b)

Yellowish white powder; Yield: (77%); m.p.: 265–267 °C. IR: υ/cm^{-1} = 3264 (NH), 3059 (CH-arom.), 2939, 2854 (CH-aliph.), 1645 (C=O), 1610 (C=N), 1341 (S=O). ^{1}H NMR: δ/ppm = 1.33 (m, 2H, piperidinyl-CH$_2$), 2.83 (t, 2H, J = 4 Hz, piperidinyl-CH$_2$), 2.93 (t, 2H, J = 4 Hz, N-CH$_2$), 3.40 (d, 2H, J = 5Hz, N-CH$_2$), 4.35 (m, 2H, piperidinyl-CH), 6.59 (d, 2H, J = 8 Hz, Ar-H), 7.08 (d, 2H, J = 8 Hz, Ar-H), 7.29 (d, 1H, J = 8 Hz, indolinone-C$_7$-H), 7.80 (s, 1H, indolinone-C$_4$-H), 8.20 (d, 1H, J = 8 Hz, indolinone-C$_6$-H), 11.41(s, 1H, NH exchangeable with D$_2$O). ^{13}C NMR: δ/ppm = 23.25, 25.37, 31.29, 35.77, 46.88 (piperidinyl-C), 111.44, 112.46, 119.79, 120.81, 121.21, 129.88, 131.60, 131.91, 134.75, 146.17 (Ar-C&CF$_3$), 157.26 (C=N), 162.77 (C=O). Mass spectrum exhibited a molecular ion peak at m/z: 455 (M$^+$, 10.38%) with a base peak at m/z: 284. Anal.Calc. for C$_{20}$H$_{17}$F$_4$N$_3$O$_3$S (455.43): C, 52.75; H, 3.76; N, 9.23. Found: C, 52.88; H, 3.66; N, 9.13.

9-((3-(Trifluoromethyl)piperidin-1-yl)sulfonyl)-6H-indolo[2,3-b]quinoxaline (7)

A solution of ethanol (20 mL) containing acetic acid (5 mL), isatin derivative 1 (0.01 mol), and *o*-phenylendiamine (0.01 mol) were added, and all of the mixture was heated under reflux for 4 h. Following the cooling of the reaction mixture to room temperature, the precipitated solid was filtered and crystallized from the acetic acid.

Red powder; Yield: (76%); m.p.: 228–230 °C IR: υ/cm^{-1} = 3263(NH), 3049 (CH-arom.), 2947, 2855 (CH-aliph.), 1609 (C=N), 1321 (S=O). ^{1}H NMR: δ/ppm = 1.33 (m, 2H, piperidinyl-CH$_2$), 2.83 (t, 2H, J = 4 Hz, piperidinyl-CH$_2$), 2.92(t, 2H, J = 4 Hz, N-CH$_2$), 3.00 (d, 2H, J = 5Hz, N-CH$_2$), 3.70 (m, 2H, piperidinyl-CH), 6.90 (d, 2H, J = 8 Hz, Ar-H), 7.26 (t, 2H, J = 8 Hz, Ar-H), 7.40 (d, 1H, J = 8 Hz, indolinone-C$_7$-H), 7.81 (s, 1H, indolinone-C$_4$-H), 8.61 (d, 1H, J = 8 Hz, indolinone-C$_6$-H), 12.49(s, 1H, NH exchangeable with D$_2$O). ^{13}C NMR: δ/ppm = 23.26, 24.99, 32.62, 43.41, 47.17 (piperidinyl-C), 115.30, 115.94, 119.79, 123.64, 128.13, 130.57, 131.29, 131.60, 132.62, 146.56, 152.47, 154.83 (Ar-C&CF$_3$), 154.77, 155.04 (2 C=N). Mass spectrum exhibited a molecular ion peak at m/z: 435 (M$^+$, 21.20%) with a base peak at m/z: 409. Anal.Calc. for C$_{20}$H$_{17}$F$_3$N$_4$O$_2$S (434.44): C, 55.29; H, 3.94; N, 12.90. Found: C, 55.21; H, 4.11; N, 12.91.

3-((4-Aminophenyl)imino)-5-((3-(trifluoromethyl)piperidin-1-yl)sulfonyl)indolin-2-one (8)

P-phenylendiamine (0.01mol) was added to a solution of compound 1 (0.01mol) in ethanol/acetic acid (20/5 mL). The mixture was heated under reflux for 4 h, and the solid result was filtered and crystallized from the acetic acid.

Dark brown powder; Yield: (83%); m.p.: 255–257 °C. IR: υ/cm^{-1} = 3455, 3180 (br. NH$_2$ & NH), 3033 (CH-arom.), 2949, 2855 (CH-aliph.), 1690 (C=O), 1611 (C=N), 1322 (S=O).^{1}H NMR: δ/ppm = 1.37 (m, 2H, piperidinyl-CH$_2$), 2.70 (t, 2H, J = 4 Hz, piperidinyl-CH$_2$), 2.86 (t, 2H, J = 4 Hz, N-CH$_2$), 2.95 (d, 2H, J = 5Hz, N-CH$_2$), 3.35 (m, 2H, piperidinyl-CH), 6.91 (d, 2H, J = 8 Hz, Ar-H), 7.03 (d, 2H, J = 8 Hz, Ar-H), 7.30 (d, 1H, J = 8 Hz, indolinone-C$_7$-H), 7.81 (s, 1H, indolinone-C$_4$-H), 8.81 (d, 1H, J = 8 Hz, indolinone-C$_6$-H), 11.41, 11.88 (2s, 3H, NH&NH$_2$ exchangeable with D$_2$O).^{13}C NMR: δ/ppm = 14.90, 23.64, 31.58, 37.82, 46.87 (piperidinyl-C), 111.84, 113.57, 118.06, 121.21, 126.73, 128.46, 129.87, 130.59, 133.33,

138.21, 143.73, 145.86 (Ar-C&CF_3), 153.10 (C=N), 162.86 (C=O). Mass spectrum exhibited a molecular ion peak at *m/z*: 453 (M^{+1}, 6.77%) with a base peak at *m/z*: 367.Anal.Calc. for $C_{20}H_{19}F_3N_4O_3S$ (452.45): C, 53.09; H, 4.23; N, 12.38.Found: C, 53.26; H, 4.14; N, 12.52.

3-((4-((4-Aminophenyl)sulfonyl)phenyl)imino)-5-((3-(trifluoromethyl)piperidin-1-yl)-sulfonyl)indolin-2-one (9)

In ethanol/acetic acid (20/5 mL), equimolar amount of 1 (0.01 mol) and Dapson (0.01 mol) were dissolved. The reaction mixture was heated under reflux for 4 h. The acetic acid-derived product dried and crystallized after being allowed to cool to room temperature.

Red powder; Yield: (67%); m.p.: 150–152 °C. IR: υ/cm^{-1} = 3371, (NH_2), 3255 (NH), 3052 (CH-arom.), 2941, 2865 (CH-aliph.), 1688 (C=O), 1594 (C=N), 1300 (S=O). ^1H NMR: δ/ppm = 1.47 (m, 2H, piperidinyl-CH_2), 2.81 (t, 2H, *J* = 4 Hz, piperidinyl-CH_2), 2.87 (t, 2H, *J* = 4 Hz, N-CH_2), 2.93 (d, 2H, *J* = 5Hz, N-CH_2), 3.30 (m, 2H, piperidinyl-CH), 5.90 (s, 2H, NH_2 exchangeable with D_2O), 6.10 (d, 2H, *J* = 8 Hz, Ar-H), 6.47 (d, 2H, *J* = 8 Hz, Ar-H), 7.03 (d, 2H, *J* = 8 Hz, Ar-H), 7.23 (d, 2H, *J* = 8 Hz, Ar-H), 7.42 (d, 1H, *J* = 8 Hz, indolinone-C_7-H), 7.52 (s, 1H, indolinone-C_4-H), 8.01 (d, 1H, *J* = 8 Hz, indolinone-C_6-H), 11.44 (s, 1H, NH exchangeable with D_2O). ^{13}C NMR: δ/ppm = 18.04, 24.67, 34.04, 38.22, 47.18 (piperidinyl-C), 111.45,116.32,116.64, 117.35, 117.75, 119.09, 122.54, 124.68, 128.86, 129.87, 133.02, 133.65, 140.98, 146.17, 146.56, 147.59, 151.37 (Ar-C&CF_3), 154.20 (C=N), 164.60 (C=O). Mass spectrum exhibited a molecular ion peak at *m/z*: 592 (M^+, 15.66%) with a base peak at *m/z*: 409. Anal.Calc. for $C_{26}H_{23}F_3N_4O_5S_2$ (592.61): C, 52.70; H, 3.91; N, 9.45. Found: C, 52.84; H, 4.11; N, 9.52.

4.2. Biological Evaluation

4.2.1. Cell Lines and Viruses

African green monkey kidney cells (VERO) and Madine Darby Canine Kidney cells (MDCK) were subcultured biweekly using Dulbecco's modified Eagle's medium (DMEM) (Lonza, Verviers, Belgium). The medium was supplemented with 10% Fetal bovine serum (Gibco, New York, NY, USA) and 1% antibiotic antimycotic mix (Lonza, Verviers, Belgium and incubated at 37 °C and 5% CO_2. Influenza A virus A/PR/8/34, HSV 1, Coxsackievirus B3 were obtained from Center of Scientific Excellence for influenza virus.

Influenza A virus was propagated in MDCK cell line, while HSV 1 and Coxsackievirus B3 were propagated in VERO cells. Viral titration via $TCID_{50}$ assay was carried out as described by Reed and Muench [58].

4.2.2. Cytotoxicity Assay

The materials and full methodology of the cytotoxicity assay of the synthesized compounds were carried out as described by Feoktistova et al. and were illustrated in detail in Supplementary Material S2 [59].

4.2.3. Antiviral Activity Assay (Inhibitory Concentration 50 Detection)

The materials and full methodology of the antiviral activity assay of the synthesized compounds were carried out as described by Mostafa et al. with little modification. The materials and full methodology were illustrated in detail in Supplementary Material S3 [60]. The IC_{50} value of each compound was calculated via non-linear regression analysis using Graphpad prism software. This was achieved by blotting log concentration of the compound versus the normalized response (variable slope) [59].

4.2.4. Quantitative PCR (qPCR)

Quantitative PCR was conducted to validate the antiviral activity (IC_{50}) results. After 72 h of incubation, cell culture lysate of cells treated with virus only (virus control), cells not treated with neither virus nor compound (cell control), and cells treated with both virus and compound were taken (the concentrations of the compounds used in the treatment was $\frac{1}{2}$ CC_{50}). Briefly, the plates were thawed and frozen 2 times. Then, the floor of

each well was scrabbed using a sterile pipette tip, and all the contents of the well were aspirated into a sterile 2 mL tube. Extraction of the nucleic acid was performed (DNA in case of HSV-1 and RNA in case of COX-B3 and influenza viruses). The principles and full methodologies for purification of total (RNA/DNA), determining the (RNA/DNA) yield, C-DNA synthesis in case of influenza and COX- B3 viruses, and qPCR reaction preparation were illustrated in detail in Supplementary Material S4. The primers used for H1N1 were; **5′-GCCAGTGGGTACGACTTTGA-3′** and **5′-CTCTTGGGACCACCTTCGTC-3′**. For HSV-1, the primers used were **5′-ATCACGGTAGCCCGGCCGTGTGACA-3′** and **5′-CATACCGGAACGCACCACACAA-3′** [61]. For COX-B3 virus, upstream primer, **5′-CAAGCACTTCTGTTTCCCCGG-3′**, and downstream primer, **5′-ATTGTCACCATAAG-CAGCCA-3′** were used [62]. Relative quantitation of target gene was estimated using $2^{-\Delta\Delta ct}$ of target gene and housekeeping gene according to the method described by Livak and Schmittgen [63].

4.3. In Silico Studies

4.3.1. Docking Studies

Molecular Docking

The antiviral activity of the synthesized 5-((3-(trifluoromethyl)piperidin-1-yl)sulfonyl)-indoline-2,3-dione derivatives (**1**–**9**) were pursued via molecular docking as well using MOE 2019 suite [64] to gain far deeper understanding of the affinities of these compounds to the active sites of the investigated viruses (H1N1 influenza virus, HSV, and Coxsackievirus B3).

Preparation of the Synthesized Derivatives (**1**–**9**)

The chemical structures of the synthesized compounds were drawn with the aid of PerkinElmer ChemOffice Suite 2017 to make them ready for the prepared docking protocol as previously described [37,65–71]. The pursued derivatives, along with their corresponding co-crystallized ligand or reference control at each active site were collected at one database as an MDB extension file to be ready for the docking protocol.

Preparation of the Virus Polymerase Active Site

The X-ray structure of the polymerases of H1N1 influenza virus, HSV, and Coxsackievirus B3 were selected carefully and downloaded from protein data bank website with **PDB entries**: **5fdd** [72], **7luf** [73], and **3ddk** [74], respectively. The molecular docking was carried out at the same active site of the co-crystallized ligand for H1N1 influenza and HSV. However, the docking was carried out at dummy site of the largest pocket of Coxsackievirus B3 since it lacks a co-crystallized inhibitor. For Coxsackievirus B3 active site molecular docking, Amiloride was selected as a reference control drug due to its reported activity as a competitive inhibitor of Coxsackievirus B3 [75]. Consequently, the protein active site of each virus was prepared for the docking process, as previously discussed in detail [65,76].

4.3.2. In Silico ADME Prediction

The anticipation of the physicochemical properties and pharmacokinetic features of the synthesized compounds (**1**–**9**) were conducted employing the online Swissadme web tool (http://www.swissadme.ch/ accessed on 20 March 2023).

Supplementary Materials: The following supporting information can be downloaded at: https://www.mdpi.com/article/10.3390/ph16091247/s1. Table S1: Cytotoxicity assay, and antiviral activity for H1N1; Table S2: Cytotoxicity assay, and antiviral activity for HSV-1 Table S3: Cytotoxicity assay, and antiviral activity for COX-B3; Table S4: The binding scores, amino acid interactions, and RMSD values of the synthesized antimicrobial candidates (**1**–**9**) at the polymerases of H1N1 influenza, HSV, and Coxackie 3b viruses along with the co-crystallized inhibitor and reference control. Table S5: The binding scores, amino acid interactions, and RMSD values of the synthesized antimicrobial candidates (**1**–**9**) at the polymerases of H1N1 influenza, HSV, and Coxackie 3b viruses along with the co-crystallized inhibitor and reference control. Figure S1: the relative gene expression levels for the

investigated samples. Figure S2: The native co-crystallized ligand (light green) and the re-docked co-crystallized ligand (simon) 3D superimposition at H1N1 RNA polymerase target protein with PDB entry: 5fdd and an RMSD value of 1.54 Å for the validation of MOE program. Figure S3: The native co-crystallized ligand (light green) and the re-docked co-crystallized ligand (simon) 3D superimposition at HSV DNA polymerase target protein with PDB entry: 7luf and an RMSD value of 1.29 Å for the validation of MOE program. Figure S4: Radar bioavailability for studied compounds in which the area in pink displays specific property optimal range. S1: Spectral Data. S2: Cytotoxicity assay. S3: Antiviral activity assay (Inhibitory concentration 50 detection). S4: qPCR methodology and principles.

Author Contributions: Conceptualization, M.A.S., A.A.A. and A.A.E.; methodology, R.R.E.E., M.A.S. and A.R.; software, R.R.E.E., H.S.E.S. and A.A.E.; validation, M.A.S., A.R. and H.S.E.S.; formal analysis, H.S.E.S. and A.A.E.; investigation, R.R.E.E., M.A.S. and A.A.E.; resources, H.S.E.S. and A.A.E.; data curation, M.A.S., A.R., R.R.E.E. and H.S.E.S.; writing—original draft preparation, M.A.S., A.A.A. and A.A.E.; writing—review and editing, R.R.E.E., S.A.A. and A.R.; visualization, A.R., M.A.S., R.R.E.E. and H.S.E.S.; supervision, M.A.S., A.A.A. and A.A.E.; project administration, R.R.E.E. and A.A.E.; funding acquisition, S.A.A. All authors have read and agreed to the published version of the manuscript.

Conflicts of Interest: The authors declare no conflict of interest.

References

1. Kausar, S.; Said Khan, F.; Ishaq Mujeeb Ur Rehman, M.; Akram, M.; Riaz, M.; Rasool, G.; Hamid Khan, A.; Saleem, I.; Shamim, S.; Malik, A. A review: Mechanism of action of antiviral drugs. *Int. J. Immunopathol. Pharmacol.* **2021**, *35*, 20587384211002621. [CrossRef]
2. Shah, B.; Modi, P.; Sagar, S.R. In silico studies on therapeutic agents for COVID-19: Drug repurposing approach. *Life Sci.* **2020**, *252*, 117652. [CrossRef] [PubMed]
3. Harvard University. World Health Statistics 2022. Available online: https://repository.gheli.harvard.edu/repository/11008/ (accessed on 22 March 2023).
4. Kondel, R.; Shafiq, N.; Kaur, I.P.; Singh, M.P.; Pandey, A.K.; Ratho, R.K.; Malhotra, S. Effect of acyclovir solid lipid nanoparticles for the treatment of herpes simplex virus (HSV) infection in an animal model of HSV-1 infection. *Pharm. Nanotechnol.* **2019**, *7*, 389–403. [CrossRef] [PubMed]
5. Waisner, H.; Kalamvoki, M. The ICP0 protein of herpes simplex virus 1 (HSV-1) downregulates major autophagy adaptor proteins sequestosome 1 and optineurin during the early stages of HSV-1 infection. *J. Virol.* **2019**, *93*, e01258-19. [CrossRef]
6. Tuddenham, S.; Hamill, M.M.; Ghanem, K.G. Diagnosis and treatment of sexually transmitted infections: A review. *JAMA* **2022**, *327*, 161–172. [CrossRef]
7. Lee, Y.-S.; Park, S.M.; Kim, B.H. Synthesis of 5-isoxazol-5-yl-2′-deoxyuridines exhibiting antiviral activity against HSV and several RNA viruses. *Bioorganic Med. Chem. Lett.* **2009**, *19*, 1126–1128. [CrossRef]
8. Biswas, B.K.; Shin, J.S.; Malpani, Y.R.; Hwang, D.; Jung, E.; Han, S.B.; Vishakantegowda, A.G.; Jung, Y.-S. Enteroviral replication inhibition by N-Alkyl triazolopyrimidinone derivatives through a non-capsid binding mode. *Bioorganic Med. Chem. Lett.* **2022**, *64*, 128673. [CrossRef] [PubMed]
9. Kaga, A.; Katata, Y.; Suzuki, A.; Otani, K.; Watanabe, H.; Kitaoka, S.; Kumaki, S. Perinatal coxsackievirus B3 infection with transient thrombocytopenia. *Tohoku J. Exp. Med.* **2016**, *239*, 135–138. [CrossRef] [PubMed]
10. Obadawo, B.; Oyeneyin, O.; Anifowose, M.; Fagbohungbe, K.; Amoko, J. QSAR evaluation of C-8-tert-butyl substituted as potent anti-enterovirus agents. *Sci. Lett.* **2020**, *8*, 28–35.
11. De Clercq, E. Strategies in the design of antiviral drugs. *Nat. Rev. Drug Discov.* **2002**, *1*, 13–25. [CrossRef]
12. Brisse, M.; Vrba, S.M.; Kirk, N.; Liang, Y.; Ly, H. Emerging concepts and technologies in vaccine development. *Front. Immunol.* **2020**, *11*, 583077. [CrossRef]
13. Salas, J.H.; Urbanowicz, R.A.; Guest, J.D.; Frumento, N.; Figueroa, A.; Clark, K.E.; Keck, Z.; Cowton, V.M.; Cole, S.J.; Patel, A.H. An antigenically diverse, representative panel of envelope glycoproteins for hepatitis C virus vaccine development. *Gastroenterology* **2022**, *162*, 562–574. [CrossRef]
14. Heida, R.; Hinrichs, W.L.; Frijlink, H.W. Inhaled vaccine delivery in the combat against respiratory viruses: A 2021 overview of recent developments and implications for COVID-19. *Expert Rev. Vaccines* **2022**, *21*, 957–974. [CrossRef] [PubMed]
15. Chiaretti, A.; Pulitanò, S.; Barone, G.; Ferrara, P.; Romano, V.; Capozzi, D.; Riccardi, R. IL-1β and IL-6 upregulation in children with H1N1 influenza virus infection. *Mediat. Inflamm.* **2013**, *2013*, 495848. [CrossRef] [PubMed]
16. Chandler, J.D.; Hu, X.; Ko, E.-J.; Park, S.; Lee, Y.-T.; Orr, M.; Fernandes, J.; Uppal, K.; Kang, S.-M.; Jones, D.P. Metabolic pathways of lung inflammation revealed by high-resolution metabolomics (HRM) of H1N1 influenza virus infection in mice. *Am. J. Physiol. -Regul. Integr. Comp. Physiol.* **2016**, *311*, R906–R916. [CrossRef] [PubMed]

17. Novoa, R.R.; Calderita, G.; Arranz, R.; Fontana, J.; Granzow, H.; Risco, C. Virus factories: Associations of cell organelles for viral replication and morphogenesis. *Biol. Cell* **2005**, *97*, 147–172. [CrossRef]

18. Jones, J.E.; Le Sage, V.; Lakdawala, S.S. Viral and host heterogeneity and their effects on the viral life cycle. *Nature Reviews Microbiology* **2021**, *19*, 272–282. [CrossRef]

19. Staufer, O.; Gantner, G.; Platzman, I.; Tanner, K.; Berger, I.; Spatz, J.P. Bottom-up assembly of viral replication cycles. *Nat. Commun.* **2022**, *13*, 6530. [CrossRef]

20. Reis, E.V.; Damas, B.M.; Mendonça, D.C.; Abrahão, J.S.; Bonjardim, C.A. In-Depth Characterization of the Chikungunya Virus Replication Cycle. *J. Virol.* **2022**, *96*, e01732-21. [CrossRef]

21. Lee, J.-Y.; Cortese, M.; Haselmann, U.; Tabata, K.; Romero-Brey, I.; Funaya, C.; Schieber, N.L.; Qiang, Y.; Bartenschlager, M.; Kallis, S. Spatiotemporal coupling of the hepatitis C virus replication cycle by creating a lipid droplet-proximal membranous replication compartment. *Cell Rep.* **2019**, *27*, 3602–3617.e5. [CrossRef]

22. Pathania, S.; Rawal, R.K.; Singh, P.K. RdRp (RNA-dependent RNA polymerase): A key target providing anti-virals for the management of various viral diseases. *J. Mol. Struct.* **2022**, *1250*, 131756. [CrossRef] [PubMed]

23. Zhu, W.; Chen, C.Z.; Gorshkov, K.; Xu, M.; Lo, D.C.; Zheng, W. RNA-dependent RNA polymerase as a target for COVID-19 drug discovery. *SLAS Discov. Adv. Sci. Drug Discov.* **2020**, *25*, 1141–1151. [CrossRef]

24. Andersen, P.I.; Ianevski, A.; Lysvand, H.; Vitkauskiene, A.; Oksenych, V.; Bjørås, M.; Telling, K.; Lutsar, I.; Dumpis, U.; Irie, Y. Discovery and development of safe-in-man broad-spectrum antiviral agents. *Int. J. Infect. Dis.* **2020**, *93*, 268–276. [CrossRef] [PubMed]

25. Singh, S.; Sk, M.F.; Sonawane, A.; Kar, P.; Sadhukhan, S. Plant-derived natural polyphenols as potential antiviral drugs against SARS-CoV-2 via RNA-dependent RNA polymerase (RdRp) inhibition: An in-silico analysis. *J. Biomol. Struct. Dyn.* **2021**, *39*, 6249–6264. [CrossRef]

26. Mouffouk, C.; Mouffouk, S.; Mouffouk, S.; Hambaba, L.; Haba, H. Flavonols as potential antiviral drugs targeting SARS-CoV-2 proteases (3CLpro and PLpro), spike protein, RNA-dependent RNA polymerase (RdRp) and angiotensin-converting enzyme II receptor (ACE2). *Eur. J. Pharmacol.* **2021**, *891*, 173759. [CrossRef] [PubMed]

27. Elsaman, T.; Mohamed, M.S.; Eltayib, E.M.; Abdel-Aziz, H.A.; Abdalla, A.E.; Munir, M.U.; Mohamed, M.A. Isatin derivatives as broad-spectrum antiviral agents: The current landscape. *Med. Chem. Res.* **2022**, *31*, 244–273. [CrossRef]

28. Ilyas, M.; Muhammad, S.; Iqbal, J.; Amin, S.; Al-Sehemi, A.G.; Algarni, H.; Alarfaji, S.S.; Alshahrani, M.Y.; Ayub, K. Insighting isatin derivatives as potential antiviral agents against NSP3 of COVID-19. *Chem. Pap.* **2022**, *76*, 6271–6285. [CrossRef]

29. El-Masry, R.M.; Al-Karmalawy, A.A.; Alnajjar, R.; Mahmoud, S.H.; Mostafa, A.; Kadry, H.H.; Abou-Seri, S.M.; Taher, A.T. Newly synthesized series of oxoindole–oxadiazole conjugates as potential anti-SARS-CoV-2 agents: In silico and in vitro studies. *New J. Chem.* **2022**, *46*, 5078–5090. [CrossRef]

30. Kumar, R.; Gideon, D.A.; Mariadasse, R.; Nirusimhan, V.; Castin, J.; Jeyakanthan, J.; Dhayabaran, V.V. In silico evaluation of isatin-based derivatives with RNA-dependent RNA polymerase of the novel coronavirus SARS-CoV-2. *J. Biomol. Struct. Dyn.* **2021**, *40*, 6710–6724.

31. Konkel, M.J.; Lagu, B.; Boteju, L.W.; Jimenez, H.; Noble, S.; Walker, M.W.; Chandrasena, G.; Blackburn, T.P.; Nikam, S.S.; Wright, J.L. 3-arylimino-2-indolones are potent and selective galanin GAL3 receptor antagonists. *J. Med. Chem.* **2006**, *49*, 3757–3758. [CrossRef]

32. Meleddu, R.; Distinto, S.; Corona, A.; Tramontano, E.; Bianco, G.; Melis, C.; Cottiglia, F.; Maccioni, E. Isatin thiazoline hybrids as dual inhibitors of HIV-1 reverse transcriptase. *J. Enzym. Inhib. Med. Chem.* **2017**, *32*, 130–136. [CrossRef]

33. Pawar, V.; Lokwani, D.; Bhandari, S.; Mitra, D.; Sabde, S.; Bothara, K.; Madgulkar, A. Design of potential reverse transcriptase inhibitor containing Isatin nucleus using molecular modeling studies. *Bioorganic Med. Chem.* **2010**, *18*, 3198–3211. [CrossRef] [PubMed]

34. Sriram, D.; Bal, T.; Yogeeswari, P. Newer aminopyrimidinimino isatin analogues as non-nucleoside HIV-1 reverse transcriptase inhibitors for HIV and other opportunistic infections of AIDS: Design, synthesis and biological evaluation. *Il Farm.* **2005**, *60*, 377–384. [CrossRef]

35. El-Demerdash, A.; Al-Karmalawy, A.A.; Abdel-Aziz, T.M.; Elhady, S.S.; Darwish, K.M.; Hassan, A.H.E. Investigating the structure–activity relationship of marine natural polyketides as promising SARS-CoV-2 main protease inhibitors. *RSC Adv.* **2021**, *11*, 31339–31363. [CrossRef] [PubMed]

36. Elebeedy, D.; Elkhatib, W.F.; Kandeil, A.; Ghanem, A.; Kutkat, O.; Alnajjar, R.; Saleh, M.A.; Abd El Maksoud, A.I.; Badawy, I.; Al-Karmalawy, A.A. Anti-SARS-CoV-2 activities of tanshinone IIA, carnosic acid, rosmarinic acid, salvianolic acid, baicalein, and glycyrrhetinic acid between computational and in vitro insights. *RSC Adv.* **2021**, *11*, 29267–29286. [CrossRef] [PubMed]

37. Elmaaty, A.A.; Alnajjar, R.; Hamed, M.I.; Khattab, M.; Khalifa, M.M.; Al-Karmalawy, A.A. Revisiting activity of some glucocorticoids as a potential inhibitor of SARS-CoV-2 main protease: Theoretical study. *RSC Adv.* **2021**, *11*, 10027–10042. [CrossRef] [PubMed]

38. Khattab, M.; Al-Karmalawy, A.A. Computational repurposing of benzimidazole anthelmintic drugs as potential colchicine binding site inhibitors. *Future Med. Chem.* **2021**, *13*, 1623–1638. [CrossRef]

39. Krämer, S.D.; Wunderli-Allenspach, H. Physicochemical properties in pharmacokinetic lead optimization. *Il Farm.* **2001**, *56*, 145–148. [CrossRef]

40. Neervannan, S. Preclinical formulations for discovery and toxicology: Physicochemical challenges. *Expert Opin. Drug Metab. Toxicol.* **2006**, *2*, 715–731. [CrossRef]
41. Müller, J.; Martins, A.; Csábi, J.; Fenyvesi, F.; Könczöl, Á.; Hunyadi, A.; Balogh, G.T. BBB penetration-targeting physicochemical lead selection: Ecdysteroids as chemo-sensitizers against CNS tumors. *Eur. J. Pharm. Sci.* **2017**, *96*, 571–577. [CrossRef]
42. Doogue, M.P.; Polasek, T.M. The ABCD of clinical pharmacokinetics. *Ther. Adv. Drug Saf.* **2013**, *4*, 5–7. [CrossRef]
43. Lipinski, C.A.; Lombardo, F.; Dominy, B.W.; Feeney, P.J. Experimental and computational approaches to estimate solubility and permeability in drug discovery and development settings. *Adv. Drug Deliv. Rev.* **1997**, *23*, 3–25. [CrossRef]
44. Ghose, A.K.; Viswanadhan, V.N.; Wendoloski, J.J. Prediction of hydrophobic (lipophilic) properties of small organic molecules using fragmental methods: An analysis of ALOGP and CLOGP methods. *J. Phys. Chem. A* **1998**, *102*, 3762–3772. [CrossRef]
45. Veber, D.F.; Johnson, S.R.; Cheng, H.-Y.; Smith, B.R.; Ward, K.W.; Kopple, K.D. Molecular properties that influence the oral bioavailability of drug candidates. *J. Med. Chem.* **2002**, *45*, 2615–2623. [CrossRef]
46. Egan, W.J.; Lauri, G. Prediction of intestinal permeability. *Adv. Drug Deliv. Rev.* **2002**, *54*, 273–289. [CrossRef] [PubMed]
47. Egan, W.J.; Merz, K.M.; Baldwin, J.J. Prediction of drug absorption using multivariate statistics. *J. Med. Chem.* **2000**, *43*, 3867–3877. [CrossRef]
48. Muegge, I.; Heald, S.L.; Brittelli, D. Simple selection criteria for drug-like chemical matter. *J. Med. Chem.* **2001**, *44*, 1841–1846. [CrossRef]
49. Daina, A.; Blatter, M.-C.; Baillie Gerritsen, V.; Palagi, P.M.; Marek, D.; Xenarios, I.; Schwede, T.; Michielin, O.; Zoete, V. Drug Design Workshop: A web-based educational tool to introduce computer-aided drug design to the general public. *J. Chem. Educ.* **2017**, *94*, 335–344. [CrossRef]
50. Daina, A.; Michielin, O.; Zoete, V. iLOGP: A simple, robust, and efficient description of n-octanol/water partition coefficient for drug design using the GB/SA approach. *J. Chem. Inf. Model.* **2014**, *54*, 3284–3301. [CrossRef]
51. Daina, A.; Michielin, O.; Zoete, V. SwissADME: A free web tool to evaluate pharmacokinetics, drug-likeness and medicinal chemistry friendliness of small molecules. *Sci. Rep.* **2017**, *7*, 42717. [CrossRef]
52. Daina, A.; Zoete, V. A boiled-egg to predict gastrointestinal absorption and brain penetration of small molecules. *ChemMedChem* **2016**, *11*, 1117. [CrossRef] [PubMed]
53. Members, S.S.I.o.B. The SIB Swiss Institute of Bioinformatics' resources: Focus on curated databases. *Nucleic Acids Res.* **2016**, *44*, D27–D37.
54. Azam, F.; Madi, A.M.; Ali, H.I. Molecular Docking and Prediction of Pharmacokinetic Properties of Dual Mechanism Drugs that Block MAO-B and Adenosine A2A Receptors for the Treatment of Parkinson's Disease. *J. Young Pharm.* **2012**, *4*, 184–192. [CrossRef]
55. Zhao, Y.H.; Abraham, M.H.; Le, J.; Hersey, A.; Luscombe, C.N.; Beck, G.; Sherborne, B.; Cooper, I. Rate-limited steps of human oral absorption and QSAR studies. *Pharm. Res.* **2002**, *19*, 1446–1457. [CrossRef]
56. Geinoz, S.; Guy, R.H.; Testa, B.; Carrupt, P.-A. Quantitative structure-permeation relationships (QSPeRs) to predict skin permeation: A critical evaluation. *Pharm. Res.* **2004**, *21*, 83–92. [CrossRef] [PubMed]
57. Delaney, J.S. ESOL: Estimating aqueous solubility directly from molecular structure. *J. Chem. Inf. Comput. Sci.* **2004**, *44*, 1000–1005. [CrossRef] [PubMed]
58. Reed, L.J.; Muench, H. A simple method of estimating fifty per cent endpoints. *Am. J. Epidemiol.* **1938**, *27*, 493–497. [CrossRef]
59. Feoktistova, M.; Geserick, P.; Leverkus, M. Crystal violet assay for determining viability of cultured cells. *Cold Spring Harb. Protoc.* **2016**, *2016*, prot087379. [CrossRef]
60. Mostafa, A.; Kandeil, A.; AMM Elshaier, Y.; Kutkat, O.; Moatasim, Y.; Rashad, A.A.; Shehata, M.; Gomaa, M.R.; Mahrous, N.; Mahmoud, S.H. FDA-approved drugs with potent in vitro antiviral activity against severe acute respiratory syndrome coronavirus 2. *Pharmaceuticals* **2020**, *13*, 443. [CrossRef]
61. Aurelius, E.; Johansson, B.; Sköldenberg, B.; Forsgren, M. Encephalitis in immunocompetent patients due to herpes simplex virus type 1 or 2 as determined by type-specific polymerase chain reaction and antibody assays of cerebrospinal fluid. *J. Med. Virol.* **1993**, *39*, 179–186. [CrossRef]
62. Leparc, I.; Aymard, M.; Fuchs, F. Acute, chronic and persistent enterovirus and poliovirus infections: Detection of viral genome by seminested PCR amplification in culture-negative samples. *Mol. Cell. Probes* **1994**, *8*, 487–495. [CrossRef] [PubMed]
63. Livak, K.J.; Schmittgen, T.D. Analysis of relative gene expression data using real-time quantitative PCR and the $2^{-\Delta\Delta CT}$ method. *Methods* **2001**, *25*, 402–408. [CrossRef] [PubMed]
64. Chemical Computing Group Inc. Molecular Operating Environment (MOE). 2016. Available online: https://www.chemcomp.com (accessed on 20 March 2023).
65. Elmaaty, A.A.; Darwish, K.M.; Khattab, M.; Elhady, S.S.; Salah, M.; Hamed, M.I.; Al-Karmalawy, A.A.; Saleh, M.M. In a search for potential drug candidates for combating COVID-19: Computational study revealed salvianolic acid B as a potential therapeutic targeting 3CLpro and spike proteins. *J. Biomol. Struct. Dyn.* **2021**, *40*, 8866–8893. [CrossRef]
66. Abo Elmaaty, A.; Hamed, M.I.; Ismail, M.I.; Elkaeed, E.B.; Abulkhair, H.S.; Khattab, M.; Al-Karmalawy, A.A. Computational insights on the potential of some NSAIDs for treating COVID-19: Priority set and lead optimization. *Molecules* **2021**, *26*, 3772. [CrossRef]

67. Hamed, M.I.; Darwish, K.M.; Soltane, R.; Chrouda, A.; Mostafa, A.; Shama, N.M.A.; Elhady, S.S.; Abulkhair, H.S.; Khodir, A.E.; Elmaaty, A.A. β-Blockers bearing hydroxyethylamine and hydroxyethylene as potential SARS-CoV-2 Mpro inhibitors: Rational based design, in silico, in vitro, and SAR studies for lead optimization. *RSC Adv.* **2021**, *11*, 35536–35558. [CrossRef]

68. Elmaaty, A.A.; Darwish, K.M.; Chrouda, A.; Boseila, A.A.; Tantawy, M.A.; Elhady, S.S.; Shaik, A.B.; Mustafa, M.; Al-Karmalawy, A.A. In silico and in vitro studies for benzimidazole anthelmintics repurposing as VEGFR-2 antagonists: Novel mebendazole-loaded mixed micelles with enhanced dissolution and anticancer activity. *ACS Omega* **2021**, *7*, 875–899. [CrossRef] [PubMed]

69. Elebeedy, D.; Badawy, I.; Elmaaty, A.A.; Saleh, M.M.; Kandeil, A.; Ghanem, A.; Kutkat, O.; Alnajjar, R.; Abd El Maksoud, A.I.; Al-Karmalawy, A.A. In vitro and computational insights revealing the potential inhibitory effect of Tanshinone IIA against influenza A virus. *Comput. Biol. Med.* **2022**, *141*, 105149. [CrossRef] [PubMed]

70. Hammoud, M.M.; Nageeb, A.S.; Morsi, M.; Gomaa, E.A.; Elmaaty, A.A.; Al-Karmalawy, A.A. Design, synthesis, biological evaluation, and SAR studies of novel cyclopentaquinoline derivatives as DNA intercalators, topoisomerase II inhibitors, and apoptotic inducers. *New J. Chem.* **2022**, *46*, 11422–11436. [CrossRef]

71. Hammouda, M.M.; Elmaaty, A.A.; Nafie, M.S.; Abdel-Motaal, M.; Mohamed, N.S.; Tantawy, M.A.; Belal, A.; Alnajjar, R.; Eldehna, W.M.; Al-Karmalawy, A.A. Design and Synthesis of Novel Benzoazoninone Derivatives as Potential CBSIs and Apoptotic Inducers: In Vitro, In Vivo, Molecular Docking, Molecular Dynamics, and SAR Studies. *Bioorganic Chem.* **2022**, *127*, 105995. [CrossRef]

72. Fudo, S.; Yamamoto, N.; Nukaga, M.; Odagiri, T.; Tashiro, M.; Hoshino, T. Two distinctive binding modes of endonuclease inhibitors to the N-terminal region of influenza virus polymerase acidic subunit. *Biochemistry* **2016**, *55*, 2646–2660. [CrossRef]

73. Hayes, R.P.; Heo, M.R.; Mason, M.; Reid, J.; Burlein, C.; Armacost, K.A.; Tellers, D.M.; Raheem, I.; Shaw, A.W.; Murray, E. Structural understanding of non-nucleoside inhibition in an elongating herpesvirus polymerase. *Nat. Commun.* **2021**, *12*, 3040. [CrossRef]

74. Campagnola, G.; Weygandt, M.; Scoggin, K.; Peersen, O. Crystal structure of coxsackievirus B3 3Dpol highlights the functional importance of residue 5 in picornavirus polymerases. *J. Virol.* **2008**, *82*, 9458–9464. [CrossRef] [PubMed]

75. Gazina, E.V.; Smidansky, E.D.; Holien, J.K.; Harrison, D.N.; Cromer, B.A.; Arnold, J.J.; Parker, M.W.; Cameron, C.E.; Petrou, S. Amiloride is a competitive inhibitor of coxsackievirus B3 RNA polymerase. *J. Virol.* **2011**, *85*, 10364–10374. [CrossRef] [PubMed]

76. Saleh, M.A.; Elmaaty, A.A.; El Saeed, H.S.; Saleh, M.M.; Salah, M.; Eldin, R.R.E. Structure based design and synthesis of 3-(7-nitro-3-oxo-3, 4-dihydroquinoxalin-2-yl) propanehydrazide derivatives as novel bacterial DNA-gyrase inhibitors: In-vitro, In-vivo, In-silico and SAR studies. *Bioorganic Chem.* **2022**, *129*, 106186. [CrossRef] [PubMed]